Am J Cancer Res 2024;14(1):324-343
www.ajcr.us /ISSN:2156-6976/ajcr0149718

Original Article

A novel immunogenic cell death-related gene risk signature can identify biomarkers of gliomas and predict the immunotherapeutic response

Xuewu Tang[1,2*], Kan Wang[3*], Jinchao Yang[1,2*], Yuting Wang[2*], Zhiteng Yan[1]

[1]Longgang District Maternity and Child Healthcare Hospital of Shenzhen City (Longgang Maternity and Child Institute of Shantou University Medical College), Shenzhen, Guangdong, China; [2]Department of Hematology and Oncology, Shenzhen Children's Hospital, Shenzhen, Guangdong, China; [3]Department of Neurosurgery, Harbin Medical University, Harbin, Heilongjiang, China. [*]Co-first authors.

Received February 17, 2023; Accepted January 1, 2024; Epub January 15, 2024; Published January 30, 2024

Abstract: Immunogenic cell death (ICD) is a type of cell death that plays a pivotal role in immunity. Recent studies have identified the critical role of ICD in glioma treatment. This study aimed to use ICD-associated differentially expressed genes (ICD-DEGs) to predict survival of glioma patients. We investigated the relationship between clinical prognosis and the date-to-clinical prognosis of 1,721 glioma patients by examining the expression, methylation, and mutation status of ICD-related genes (IRGs) in these patients. Our prediction of survival in glioma patients was based on three risk genes, and we explored the association between these genes and clinical outcomes. Additionally, IRG expression was used to stratify glioma patients. We further examined the relationship among the three subgroups in terms of immune microenvironment heterogeneity and immunotherapy response. In addition, this study also included analyses of histograms and sensitivity to antitumor drugs. The expression of these genes was externally validated by RT-qPCR, Western blot (WB), and immunohistochemistry (IHC) in glioma and normal brain tissue. Our findings reveal that most IRGs are overexpressed in glioma tumor tissues, and this high expression was confirmed through histological validation. We successfully developed predictive models for three prognostic genes associated with ICD. These models not only predict survival in glioma but also correlate with the tumor's immune microenvironment. Finally, using consensus clustering, we identified three ICD-associated subtypes. Notably, patients with the C3 subtype showed high levels of immune cell infiltration, whereas those with the C1 subtype exhibited lower levels of immune cell infiltration. We successfully developed an innovative IRG-based systematic approach for evaluating glioma patients. This stratification in experimental studies opens new avenues for prognosis and assessing immunotherapy responses in glioma patients. Our study demonstrates the effectiveness of this approach in treating glioma, potentially paving the way for more promising and effective therapeutic strategies in the future.

Keywords: Glioma, immunogenic cell death (ICD), tumor microenvironment (TME), immunotherapy, drug sensitivity analysis

Introduction

Glioma, a common cancer in children and adolescents, is thought to originate from glial progenitor or stem cells [1]. However, the exact origin of most pediatric gliomas remains elusive. Pediatric gliomas exhibit distinct histological, molecular, and clinical features, emerging from specific cell populations vulnerable to oncogenic events during particular developmental phases of the central nervous system (CNS) [2]. Standard treatments for glioma include observation, surgery, chemotherapy, and radiation therapy [3]. Throughout the past few decades, significant advancements in glioma treatment have enhanced surgical procedures. However, due to the nature of the cells, the treatment of gliomas presents significant difficulties [4-6]. Recent biomarker discoveries have improved cancer patient survival and targeted antitumor treatment [5, 7]. Despite the discovery of a number of predictive biomarkers, such as lncRNA FOXD1-AS1 [8] and hemodynamic alterations, the prognosis for patients

https://doi.org/10.62347/VCFG8784

with high-grade gliomas is frequently still poor [9]. Consequently, developing more accurate predictive models and cellular targets for gliomas is critically important. This represents a key area for drug research and development.

ICD is a novel kind of regulatory cell death that can trigger adaptive immune responses. Numerous studies have thoroughly investigated the concept of immunostimulatory death [10, 11]. Owing to the heterogeneity of tumors, different tumor types have variable responses to immunotherapy. Tumors less responsive to immunotherapy are often referred to as "cold tumors", while those responsive are termed "hot tumors". Most researchers have studied how to convert cold tumors into hot tumors. Several recent studies have emphasized the significance of ICD in cancer progression and immunotherapy [12-14]. Ahmed et al. highlighted that ICD could initiate anti-cancer immune responses [15]. Nevertheless, the specific role of ICD in gliomas remains unclear. Further patient-based research is necessary to explore the potential of ICD in glioma treatment. Specifically, it would be extremely beneficial to identify biomarkers that can classify patients.

In this study, we analyzed mRNA profiles and clinical data of glioma patients from public databases. We established a prognostic gene signature based on ICD-related differentially expressed genes (ICD-DEGs) using data from The Cancer Genome Atlas (TCGA) group and validated its predictive efficacy in the Chinese Glioma Genome Atlas (CGGA) group. A clinical treatment-guiding model was developed to determine the prognosis of glioma patients. Finally, this model was validated for its ability to predict glioma characteristics and employed functional enrichment analysis to identify potential mechanisms of action. These insights could help clinicians devise more targeted and effective treatment strategies.

Materials and methods

Data collection

Data acquisition and analysis processes are illustrated in Supplementary Figure 1. TCGA-Lower grade glioma (TCGA-LGG) and TCGA-Glioblastoma (TCGA-GBM) pairs (n = 703) were obtained from TCGA (https://portal.gdc.cancer.GOv). For validation, patient biological data were standardized by converting expression profiles into transcript values per kilobase. Analyses were conducted using R programming language. Gencode (version 26) GTF files for mRNA annotation and differentiation were retrieved from Ensemble (http://asia.ensembl.org). Additionally, clinical information including sex, age, clinical stage, and survival was downloaded from the TCGA data portal. Patients with survival time under 30 days were excluded. Data normalization employed the "limma" package [16]. The "Deseq2" R package was then used for variance analysis (Supplementary Tables 1 and 2).

Identification of differentially expressed genes

Differentially expressed genes (DEGs) in the TCGA dataset were identified by comparing mRNA expression of 34 IRGs across tissue types. The message on the specimen source (TCGA-LGG or TCGA-GBM) was included as a covariate in this analysis. IRGs meeting the criteria ($P < 0.05$, fdr < 0.05 and |log FC| for genes > 1) were selected for further analysis.

Gene correlation analysis and functional enrichment analysis

Protein-protein interactions among DEGs were analyzed using the STRING database [17]. Gene Ontology (GO) and Kyoto Encyclopedia of Genes and Genomes (KEGG) pathway analyses were carried out in R software using Cluster Profiler [18] for the functional annotation of differentially expressed genomes to elucidate pathways and biological effects among the various groups of signaling ICDs during the investigation. GO and the KEGG route was evaluated using the R software's "Cluster Profiler" tool. GO utilized the *q-value and p-value* along with KEGG abundance analysis.

Construction and identification of ICD related signature

Univariate Cox regression analysis in the TCGA dataset identified genes significantly linked to overall survival (OS) based on IRGs. The predictive power of IRGs was evaluated using Cox regression analysis. To refine ICD-associated gene profiles, Venn diagrams identified genes shared between clinically significant genes and DEGs. These overlapping genes were then analyzed using LASSO Cox regression analysis via

the Glmnet software [19]. The entire TCGA glioma patient cohort served as the training group, while the CGGA glioma patients (n = 242) constituted the test group. We stratified the training group into two groups based on their median risk-scores for determination of prognostic risk-scores for immunogenic mortality.

Differences in OS between these two groups were investigated. Kaplan-Meier analysis (KMA) was utilized to compare OS times across these groups. Additionally, DEG-based Principal Component Analysis (PCA) was performed using a statistical package, and normalization of each DEG associated with immunogenic mortality was conducted in the test group. The model's validation was carried out using the test group, with individual patient risk-scores calculated as follows: Risk-score = (0.00019 * BAX expression level + 0.299 * CASP8 expression level + 0.0377 * MYD88 expression level).

Consensus clustering analysis of IRGs

We conducted unsupervised consensus clustering analysis using the "Consensus ClusterPlus" R package. To validate our classification's accuracy, 1000 replications were performed, categorizing patients into various molecular subtypes as per the CRG [20]. We next applied KMA to calculate survival differences across these subtypes.

Correlation of ICD related signature, genotypes and TME

For the purpose of evaluating percentage in 23 glioma immune cell subpopulations, the CIBERSORT was used. The amount of immune cell inflammation in TME of glioma patients was examined using the single sample gene set enrichment analysis (ssGSEA) algorithm [21, 22]. Additionally, the "ESTIMATE" software was employed to evaluate immune and tumor purity scores [23, 24].

Mutation single nucleotide polymorphism (SNP) and copy number variation (CNV) analysis

Glioma SNP data were analyzed using the Map Toolkit [25]. Waterfall plots featuring the top ten genes from Section 2.12 illustrated mutations in the top 20 genes, facilitating the exploration of changes in SNP presentation between two groups. Tumor mutational burden (TMB), defined as the sum of all somatic mutations per megabase in each tumor sample, was calculated by counting the mutations present in the sample. The TMB in the high/low-risk groups was then statistically evaluated. For CNV analysis, CNV files from the database were first marked and imported into the GenePattern software, followed by visualization using the Map Toolkit [25].

Establishment and validation of a nomogram and scoring system

Graphs of prediction curves were created using the "rms" software [26]. Receiver Operating Characteristic (ROC) curves were used to evaluate histograms over time. Calibration curves were used to display the differences between projected and actual outcomes.

Drug sensitivity analysis

Drug half-maximum inhibitory concentrations (IC50) were predicted using a correlation ridge regression model with the pRRophetic algorithm [27]. This model used the TCGA cohort as the evaluation data for expression profiles and the Genomics of Drug Sensitivity in Cancer (GDSC) cell line as the training data (https://www.cancerrxgene.org/). The IC50 values of various regularly used medications from the TCGA dataset were predicted in this research via studying the relationship between lncRNA expression and the IC50 values of these medicines and cisplatin using spearman correlation.

Cell culture

U251 and ln229 cell lines were acquired from Procell Life Science & Technology Corporation, located in Wuhan, China. These cell lines were cultured in Dulbecco's Modified Eagle's Medium (DMEM), sourced from HyClone, Logan, USA, supplemented with 10% fetal bovine serum (FBS) from Invitrogen, Carlsbad, CA, USA. Cells were maintained at 37°C in a 5% CO_2 atmosphere. For experimental analysis, cells were used in the logarithmic phase of growth.

Cell transfection

Lentivirus STMN1-shRNA was acquired from Genechem (Shanghai, China). The shRNA se-

quences were as follows: shRNA sequence 1: 5'-TGGCATCTGGAGATGGCAATA-3'; shRNA sequence 2: 5'-CCGCGTGGTTGCCCTCTTCTA-3'. U251 and ln229 cells were seeded at a density of 3-5×10^4 cells/ml into 6-well plates and cultured at 37°C for 16-24 hours until the cell confluence reached 30-50%. The cells were maintained under the same conditions until the desired confluence was achieved. According to provided instructions, lentivirus and infection enhancer were added to the culture. After 16 hours, the medium was replaced, and the cells were incubated further.

Collection of clinical samples

We obtained clinical samples comprising tissues from 10 glioma patients and 10 normal brain tissues obtained post-surgery for severe craniocerebral trauma between January 2021 and October 2022 at Longgang District Maternity & Child Healthcare Hospital, Shenzhen. The human tissues or specimens used in this study were obtained from previous medical records, not collected specifically for this study, and, in accordance with national medical ethical standards, can be exempt from informed consent. The tissues or specimens were used only for this study and not for other research. Excess tissues or specimens were returned at the end of the study and research results were reviewed to ensure confidentiality of personal information about the source of the tissues or specimens. The study was approved by the Ethics Committee of Shenzhen Longgang District Maternal and Child Hospital with the ethical approval number LGFYYXLLL-2022-032.

Cell viability analysis

Cells were plated in 96-well plates at a density of 2×10^3 cells per well in DMEM. Post-treatment, cells were cultured for 24 and 48 h. Ten microliters of Cell Counting Kit-8 (CCK-8) reagent (Glpbio, California, USA) was added to each well and incubated at 37°C for 1 h. The absorbance of each well was measured at 450 nm with a microplate reader.

Wound healing assay

Cells were seeded in 6-well plates at a density of 15×10^4 cells/ml. Upon reaching 80-90% confluence, a 200 µl pipette tip was used to create a scratch, followed by rinsing with PBS and incubation in DMEM without FBS. Cell migration in the wound area was photographed under a microscope at 24 h and 48 h. Wound healing was measured on the images, and the migration area was calculated by the length of the original wound minus the length of the wound during healing using ImageJ software.

Invasion assay

For the invasion study, chamber inserts were coated with 40 µl of BD Matrigel (Corning, USA) and allowed to solidify at 37°C for 1 hour. Approximately 5×10^4 cells were resuspended in 500 µl FBS-free DMEM and plated into the top chamber of the insert, which was then placed into a 24-well plate containing 750 µl FBS-containing DMEM. After 24 hours, migrated cells were fixed with 4% paraformaldehyde, stained with 0.05% crystal violet, and counted under a microscope.

Western blotting method

Post-treatment, the cells of each group were collected, washed twice with PBS, and lysed in RIPA buffer with phosphatase inhibitors in an ice water bath for 30 minutes. To assist in lysis, lysate was subject to an ultrasonic cell fragmentation apparatus. Protein concentration was detected by the BCA method after centrifugation. The denatured proteins were separated by SDS-PAGE (60 µg per well), transferred to PVDF membranes, and blocked in 5% skim milk powder for 2 hours. Membranes were incubated overnight at 4°C with primary antibodies, washed with 1× PBST 3 times, followed by a 2 h incubation with a secondary antibody (Beyotime) at room temperature. Membranes were washed with 1× PBST 3 times and visualized using an enhanced chemiluminescence kit (Beyotime, Shanghai, China). Protein bands were analyzed using ImageJ software. GAPDH was used as a reference for normalization.

Quantitative reverse transcription polymerase chain reaction (RT-qPCR)

Total RNA was extracted from tissues using TRIzol reagent (Invitrogen, Carlsbad, CA, USA). Complementary DNA was synthesized using PrimeScript RT kits (Takara, Osaka, Japan) following the manufacturer's protocol. RT-qPCR was performed with SYBR Green assay (Takara) on an ABI 7500 system (Applied Biosystems,

Waltham, USA). Primer sequences are detailed in Supplementary Table 3.

Human protein atlas database and IHC validation

Protein expression levels of TCRs-related hallmark genes in glioma samples were analyzed using the Human Protein Atlas online database (https://www.proteinatlas.org/) with integratedomics techniques [28].

Immunohistochemistry

Glioma specimens of varying grades and normal brain tissues were fixed in formalin, embedded in paraffin, and sectioned into 4-micron slices. These sections underwent deparaffinization in citrate buffer, dehydration, pretreatment for antigen recovery, and quenching of endogenous peroxidase activity using 3% hydrogen peroxide (H_2O_2). Non-specific antigenic sites were blocked with 10% normal goat serum and sections were incubated overnight at 4°C with BAX, CASP8, and MYD88 antibodies (dilutions 1:100 from Abcam and 1:500 from CST, respectively). Sections were then incubated with secondary antibody (goat anti-rabbit IgG, 1:5000, Proteintech) and stained with diaminobenzidine hydrochloride (DAB) and hematoxylin. IHC images were captured, and the fraction of protein expression was quantified using Image J.

Statistical analysis

The independent predictive power of the suggested model was examined using a Cox regression model. All statistical analyses were conducted using R version 4.1.0. Significant differences between different groups are denoted as follows: *$P < 0.05$, **$P < 0.01$, ***$P < 0.001$, ****$P < 0.0001$. The threshold for statistical significance was set at $P < 0.05$.

Results

Genetic changes and presentation of ICD-related genes in glioma

Our comprehensive analytical flow is presented in Supplementary Figure 1. Most ICDs genes, including ATG5, BAX, CALR, CASP1, CASP8, CD4, CD8B, CXCR3, EIF2AK3, HMGB1, IFNB1, IFNG, IFNGR1, IL10, IL17A, IL1R1, LY96, MYD88, NT5E, PDIA3, PRF1, and TNF, were found to be overexpressed in gliomas (**Figure 1A**). At the genomic level, 145 (14.74%) of the 984 samples revealed regulatory mutations associated with ICD, with TP53 showing the highest frequency of mutations (**Figure 1B**, **1C**). We then explored the connections between IRGs (**Figure 1F**) and used the STRING platform to investigate potential bio-functional networks linked to ICD regulators (**Figure 1D**). The Cytoscape plug-in was utilized to analyze the regulatory networks of HUB genes (**Figure 1E**). Correlations were predicted between genes within these network maps, and pathways enriched in alphabetical similarity were analyzed. We observed that processes such as interleukin-1 signaling, macrophage differentiation, antigen processing and presentation, lipids and atherosclerosis, and most ICD-associated prognostic genes were enriched for positive regulation of these processes (**Figure 1G**, **1H**). Thus, it was demonstrated that the expression levels of ICD-related genes correlated with glioma, suggesting their potential representation of various patient characteristics.

Association between prognosis and immunogenic apoptosis-associated degs in glioma

We identified 15 prognostically associated glioma ICD regulators by integrating 34 ICD-related differentially expressed genes from our study with genes linked to prognosis (**Figure 2A**). We found that the expression levels of most prognosis-related ICD regulators, including BAX, CASP1, CASP8, CALR, CD4, CD8B, CXCR3, EIF2AK3, IFNB1, IFNG, IL10, IL1R1, LY96, MYD88, and PDIA3, were associated with glioma (**Figure 2B**). Additional univariate analysis revealed 15 prognosis-related genes to be associated with poor OS in glioblastoma (**Figure 2C**). Through gene prognostic network maps, we also discovered co-expression interactions among 15 ICD regulators linking to glioma prognosis, which influenced glioma formation and progression through their reciprocal regulatory effects (**Figure 2D**, **2E**).

Construction of an immunogenic apoptosis-related gene signature model

We aimed to construct predictive models by analyzing the expression profiles of 15 genes using LASSO Cox regression. Three genes were characterized based on the optimal cutoff

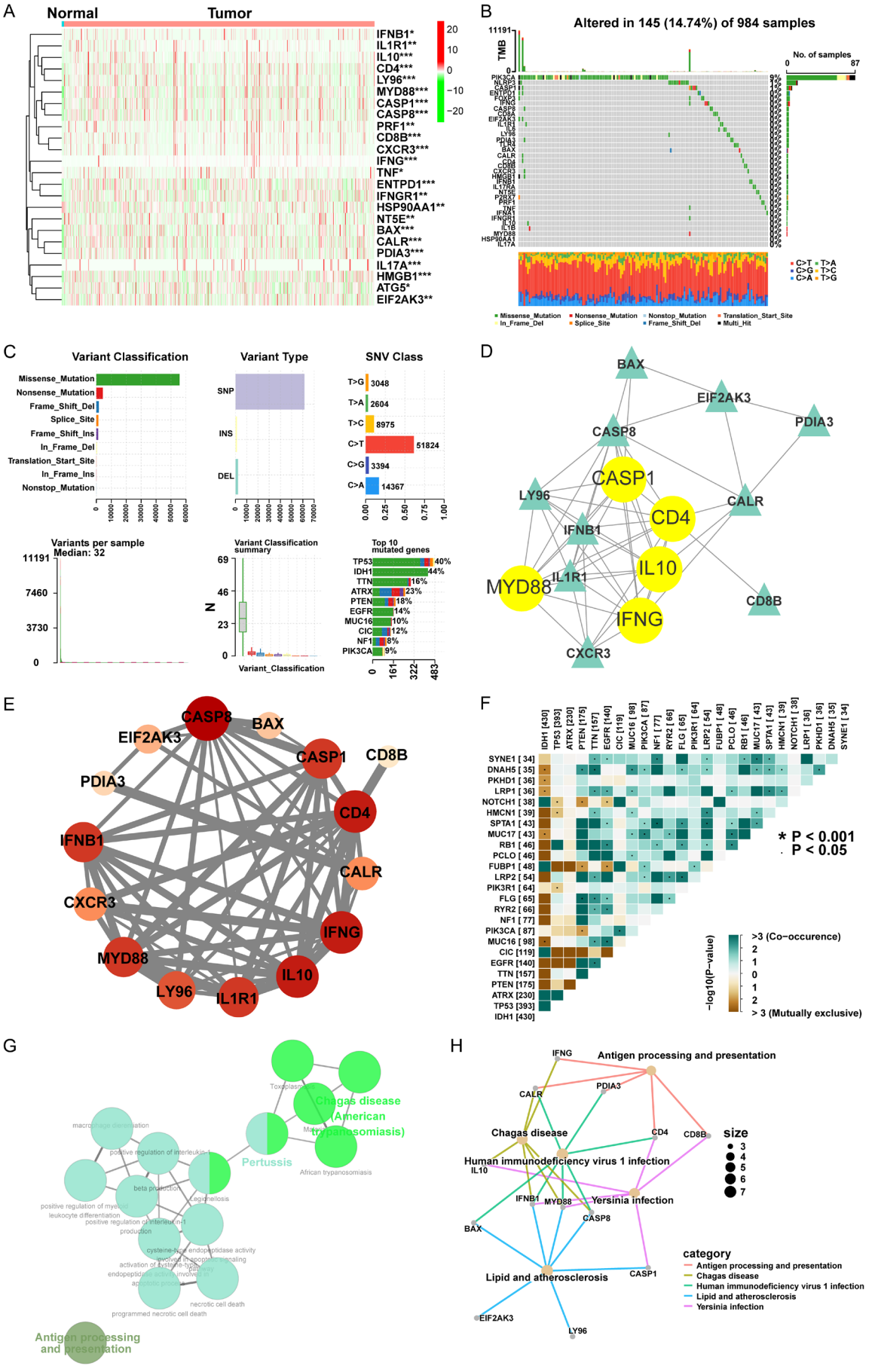
A
Normal
Tumor
IFNB1*
IL1R1**
IL10***
CD4***
LY96***
MYD88***
CASP1***
CASP8***
PRF1**
CD8B***
CXCR3***
IFNG***
TNF*
ENTPD1***
IFNGR1**
HSP90AA1**
NT5E**
BAX***
CALR***
PDIA3***
IL17A***
HMGB1***
ATG5*
EIF2AK3**
B
Altered in 145 (14.74%) of 984 samples
TMB
No. of samples
C>T T>A
C>G T>C
C>A T>G
Missense_Mutation
Nonsense_Mutation
Nonstop_Mutation
Translation_Start_Site
In_Frame_Del
Splice_Site
Frame_Shift_Del
Multi_Hit
C
Variant Classification
Missense_Mutation
Nonsense_Mutation
Frame_Shift_Del
Splice_Site
Frame_Shift_Ins
In_Frame_Del
Translation_Start_Site
In_Frame_Ins
Nonstop_Mutation
Variant Type
SNP
INS
DEL
SNV Class
T>G 3048
T>A 2604
T>C 8975
C>T 51824
C>G 3394
C>A 14367
Variants per sample
Median: 32
Variant Classification summary
Variant_Classification
Top 10 mutated genes
TP53 40%
IDH1 44%
TTN 16%
ATRX 23%
PTEN 18%
EGFR 14%
MUC16 10%
CIC 12%
NF1 8%
PIK3CA 9%
D
BAX
EIF2AK3
PDIA3
CASP8
CASP1
LY96
CALR
CD4
IFNB1
IL10
IL1R1
MYD88
CD8B
IFNG
CXCR3
E
CASP8
BAX
EIF2AK3
CASP1
CD8B
PDIA3
CD4
IFNB1
CALR
CXCR3
IFNG
MYD88
IL10
LY96
IL1R1
F
IDH1 [430]
TP53 [393]
ATRX [230]
PTEN [175]
TTN [157]
EGFR [140]
CIC [119]
MUC16 [98]
PIK3CA [87]
NF1 [77]
RYR2 [66]
FLG [65]
PIK3R1 [64]
LRP2 [54]
FUBP1 [48]
PCLO [46]
RB1 [46]
MUC17 [43]
SPTA1 [43]
HMCN1 [39]
NOTCH1 [38]
LRP1 [36]
PKHD1 [36]
DNAH5 [35]
SYNE1 [34]
* P < 0.001
. P < 0.05
−log10(P−value)
>3 (Co−occurence)
> 3 (Mutually exclusive)
G
Chagas disease (American trypanosomiasis)
Pertussis
African trypanosomiasis
Toxoplasmosis
Legionellosis
necrotic cell death
programmed necrotic cell death
Antigen processing and presentation
H
IFNG
Antigen processing and presentation
CALR
PDIA3
Chagas disease
CD4
CD8B
Human immunodeficiency virus 1 infection
IL10
IFNB1
MYD88
Yersinia infection
CASP8
BAX
Lipid and atherosclerosis
CASP1
EIF2AK3
LY96
size
category
Antigen processing and presentation
Chagas disease
Human immunodeficiency virus 1 infection
Lipid and atherosclerosis
Yersinia infection

Figure 1. Characterization and differences of ICD-associated regulators in gliomas. A: Heat map showed 24 ICD gene expression profiles in normal and glioma samples from the TCGA database. B: Mutation profiles of 984 glioma patients from the TCGA-GBM cohort and TCGA-LGG. Each waterfall plot represents mutational information for each focal death-associated regulator. Corresponding colors are annotated at the bottom to indicate the different mutation types. The top bar graph shows the mutation burden. The correct numbers represent the mutation frequencies. C: Shows the different classifications of ICD-associated regulators and CNV frequencies, respectively. The height of the bars shows the proportion of different types. D, E: Collection of potential biological interactions of ICD-associated regulators from the STRING platform. F: The plot of correlation analysis between ICD-associated genes. Indicates $P < 0.05$, *indicates $P < 0.001$. G, H: Gene function enrichment analysis of ICD-associated genes by Cytoscape plug-in.

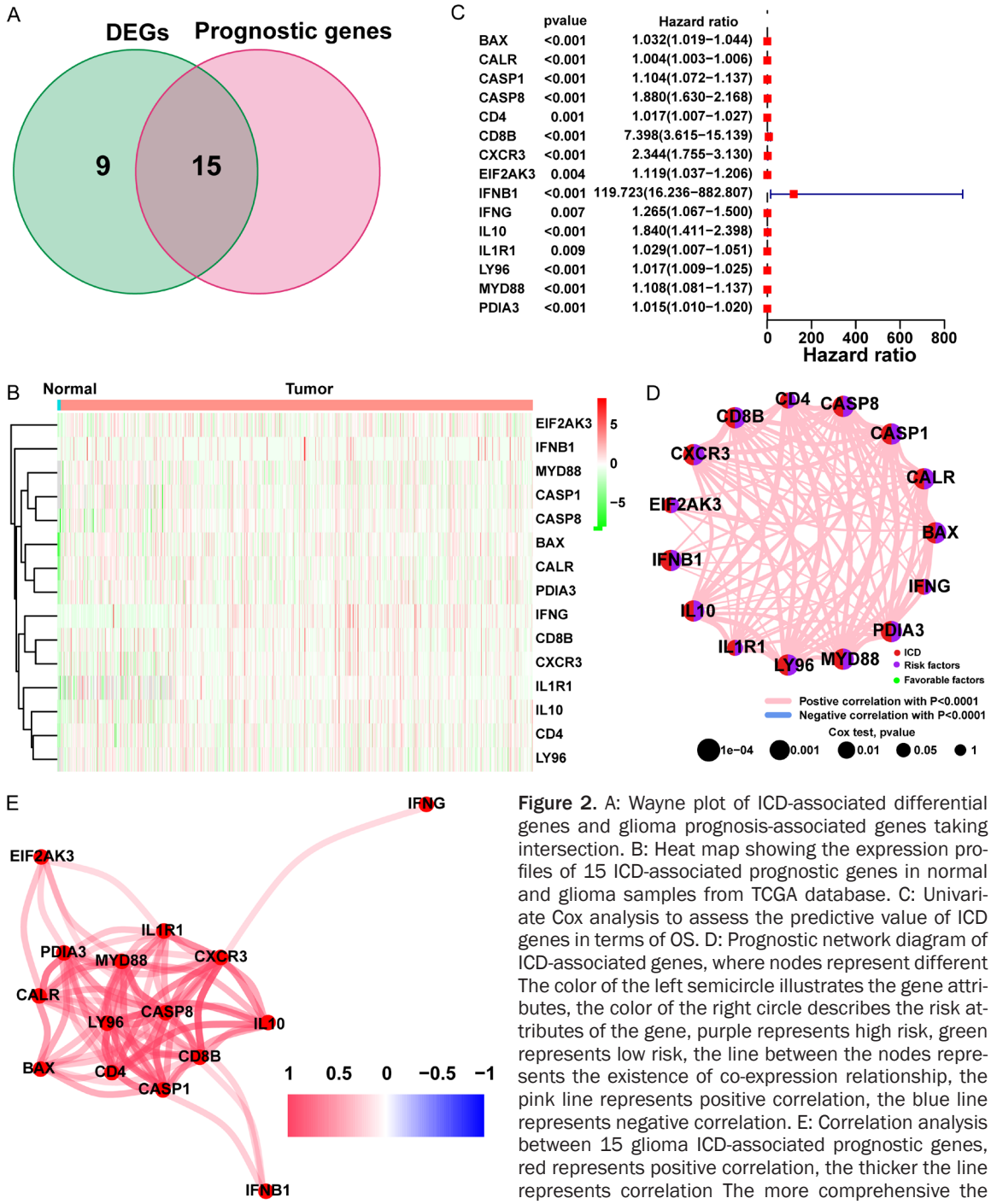

Figure 2. A: Wayne plot of ICD-associated differential genes and glioma prognosis-associated genes taking intersection. B: Heat map showing the expression profiles of 15 ICD-associated prognostic genes in normal and glioma samples from TCGA database. C: Univariate Cox analysis to assess the predictive value of ICD genes in terms of OS. D: Prognostic network diagram of ICD-associated genes, where nodes represent different The color of the left semicircle illustrates the gene attributes, the color of the right circle describes the risk attributes of the gene, purple represents high risk, green represents low risk, the line between the nodes represents the existence of co-expression relationship, the pink line represents positive correlation, the blue line represents negative correlation. E: Correlation analysis between 15 glioma ICD-associated prognostic genes, red represents positive correlation, the thicker the line represents correlation The more comprehensive the line, the stronger the correlation.

value, where high expression was associated with unfavorable outcomes in our previous analysis (all adjusted *P * 0.05*, **Figure 3A**, **3B**). The risk scores were calculated as follows: Risk-core = (0.00019 * expression levels of BAX, CASP8, and MYD88 + 0.299 * expression levels of BAX). Patients were stratified into high-risk (n = 315) and low-risk (n = 316) groups based on the median critical value. In the TCGA cohort, high-risk patients exhibited a higher mortality rate, demonstrating that the overall survival (OS) of the high-risk group was significantly lower than that of the low-risk group (**Figure 3C**, *P < 0.001*). Surprisingly, progression-free survival (PFS) was also significantly lower in the high-risk group compared to the low-risk group (**Figure 3E**). ROC analysis of the risk-score yielded areas under the curve (AUC) values of 0.736 (1 year), 0.690 (2 years), and 0.710 (3 years) (**Figure 3D**). PCA and tSNE were utilized to illustrate the bivariate distributions for patients in different risk groups (**Figure 3F**, **3G**). Overall, the signature proposed in this study emerged as a valuable predictive model for glioma patient risk classification.

Additionally, we conducted a similar analysis using the external validation cohort from CGGA to enhance the reliability of our study's model. Patients were categorized into high-risk (n = 721) and low-risk (n = 244) groups based on median cutoff values. High-risk patients generally had shorter survival periods than those in the low-risk group (Supplementary Figure 2A, 2B). Kaplan-Meier curves for the CGGA validation group confirmed that OS in the high-risk group was significantly lower than that in the low-risk group (Supplementary Figure 2C).

ROC curves plotted using the CGGA validation data revealed AUC values of 0.693, 0.744, and 0.766 for 1, 2, and 3-year survival periods, respectively (Supplementary Figure 2D). PCA and tSNE analyses further divided the CGGA validation cohort into two groups (Supplementary Figure 2E, 2F). These findings indicated that the validation outcomes in the CGGA cohort were consistent with those in the TCGA training cohort, further affirming that our signature is a robust prognostic model.

Clinical characterization of differential genetic profiles associated with immunogenic apoptosis in low- and high-risk populations

Next, we sought to explore the potential of ICD for clinical application, particularly its utility in predicting the prognosis of glioma patients. To this end, we utilized a column line plot, integrating three readily accessible clinical features commonly believed to influence glioma prognosis, along with the risk score's capacity to predict patients' 1, 3, and 5-year survival rates (**Figure 4B**, **4D**). The column line plots demonstrated robust predictive values, as indicated by a C-index of 0.736 (**Figure 4C**). Further analysis revealed significant associations in the high-risk group with various factors, including higher tumor grade, advanced age, and increased risk score (**Figure 4A**).

Functional enrichment analysis of differentially expressed genes in low and high-risk groups

Functional enrichment analysis of the differentially expressed genes in the high-risk and low-risk groups was conducted using the "Limma" R package. In terms of biological processes (BPs), IRGs were predominantly enriched in leukocyte-mediated immunity, lymphocyte-mediated immunity, immunoglobulin-mediated immune response, and B-cell activities. For cellular components (CCs), enrichment was primarily observed in the extracellular matrix, including collagen, collagen trimers, and major histocompatibility complex (MHC) class II proteins. For molecular functions (MFs), IRGs were mostly enriched in extracellular matrix structural components, MHC protein complex binding, collagen-related genes, and T-cell activation. Tensile strength is conferred via collagen binding, MHC protein complex binding, MHC class II protein complex binding, and structural elements of the extracellular matrix (Supplementary Figure 3A, 3C). The KEGG pathways enriched in IRGs were analyzed using the DAVID online tool and visualized with R. IRGs were found to be abundant in pathways related to type I diabetes, Staphylococcus aureus infection, viral myocarditis, and interactions between the ECM and receptors (Supplementary Figure 3B, 3D).

Somatic mutations and tumor microenvironment landscape in ICD-high and ICD-low subtypes

Given the growing evidence of ICD's importance in eliciting specific anti-tumor immune responses, we compared the TME composition between high and low-risk groups. High-risk patients generally exhibited higher percentages of B cells, CD8 T cells, activated bone marrow den-

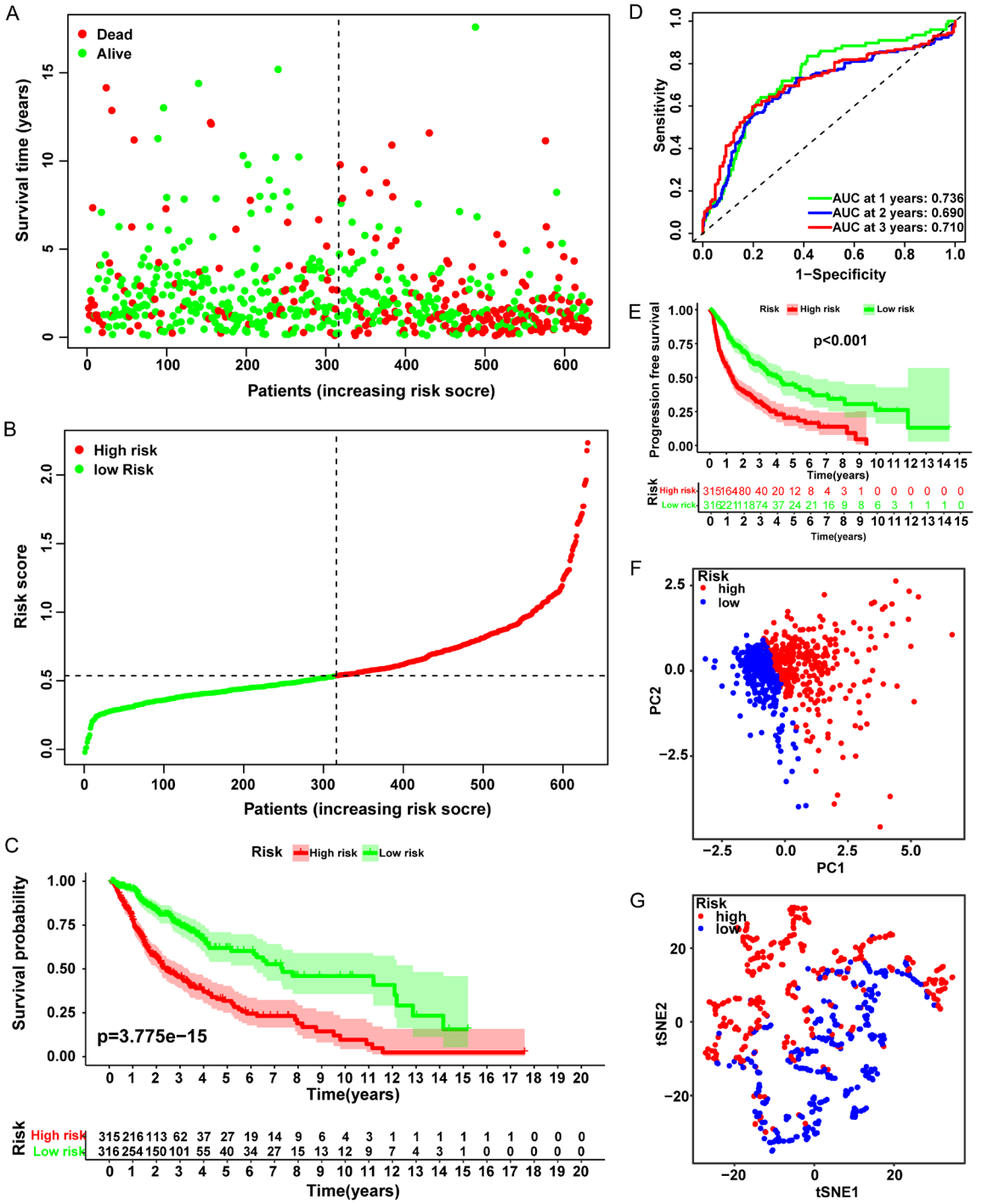

Figure 3. Validation of ICD-associated risk model prediction results in the TCGA dataset. A: The risk score of each patient. B: Survival outcomes for each patient. C: Kaplan-Meier curves are based on overall survival for high-risk and low-risk patients. D: 1-year, 2-year, and 3-year ROC curves derived from optimized model construction show all AUC values above 0.65. E: Kaplan-Meier curves are based on progression-free survival in high- and low-risk patients. F: PCA results indicated a significant difference in transcriptional expression between the two isoforms. G: The results of tSNE similarly showed the transcriptional expression of these two genes. There was good discrimination between the homozygotes.

dritic cells, macrophages M1 and M2, and regulatory T cells (**Figure 5B**). Increased expression of most human leukocyte antigen (HLA) genes and immune checkpoints was observed in the

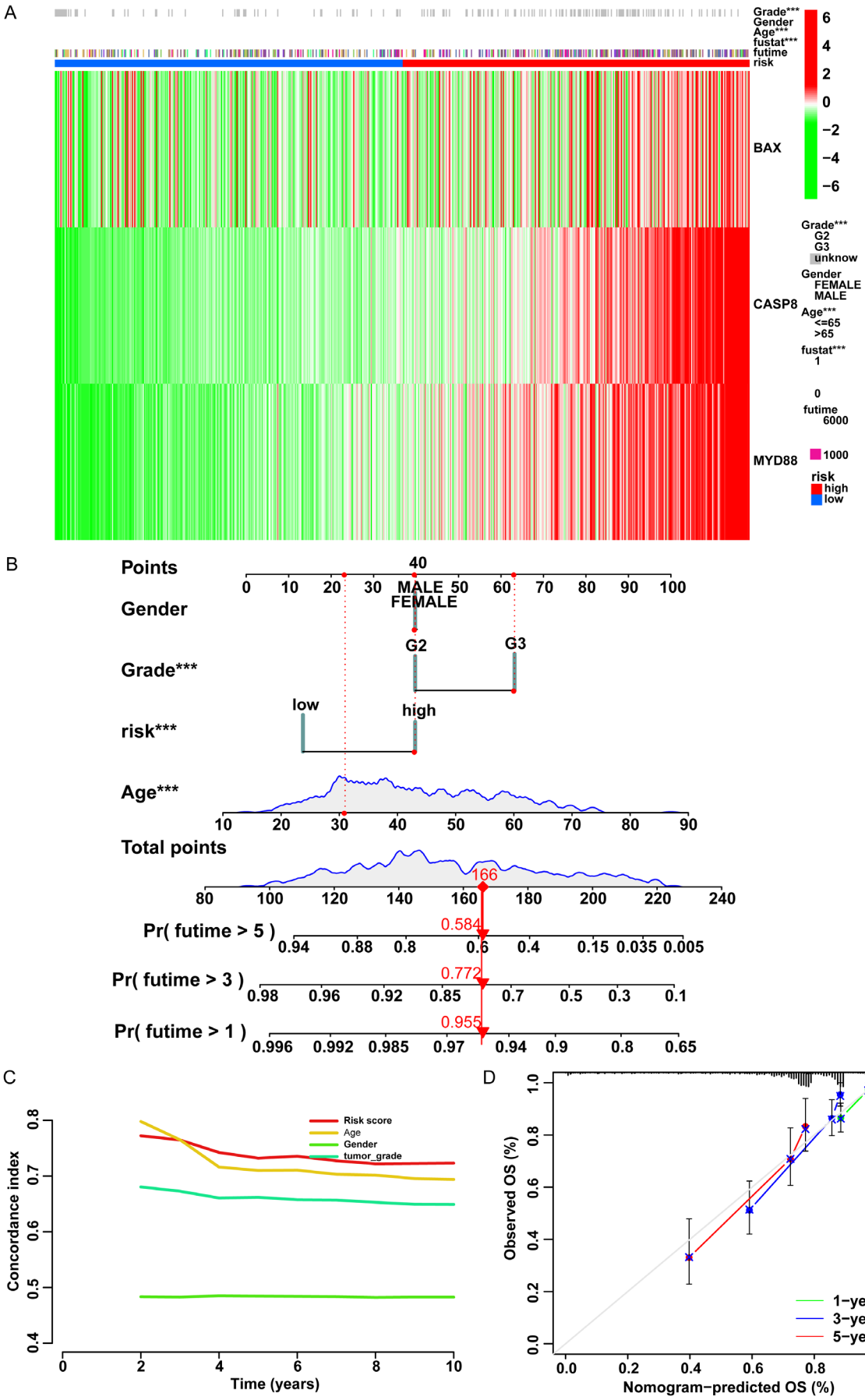
A
Grade***
Gender
Age***
fustat***
futime
risk
BAX
CASP8
MYD88
6
4
2
0
−2
−4
−6
Grade***
G2
G3
unknow
Gender
FEMALE
MALE
Age***
<=65
>65
fustat***
1
0
futime
6000
1000
risk
high
low
B
Points
Gender
Grade***
risk***
Age***
Total points
Pr(futime > 5)
Pr(futime > 3)
Pr(futime > 1)
MALE
FEMALE
G2
G3
low
high
166
0.584
0.772
0.955
C
Concordance index
Time (years)
Risk score
Age
Gender
tumor_grade
D
Observed OS (%)
Nomogram−predicted OS (%)
1−year
3−year
5−year

Figure 4. Establishment of a prediction nomogram for immunogenic cell death-related genes in gliomas. A: Heat map showing the unsupervised clustering of 3 IRGs associated with glioma prognosis in the glioma cohort. B: Immunogenic cell death-related genes predictive nomogram predicted 1, 3, and 5 years OS in glioma patients. C: The DCA of the risk factors. D: Calibration curves for immunogenic cell death-related prediction nomograms for predicting 1-year, 3-year, and 5-year OS in glioma patients.

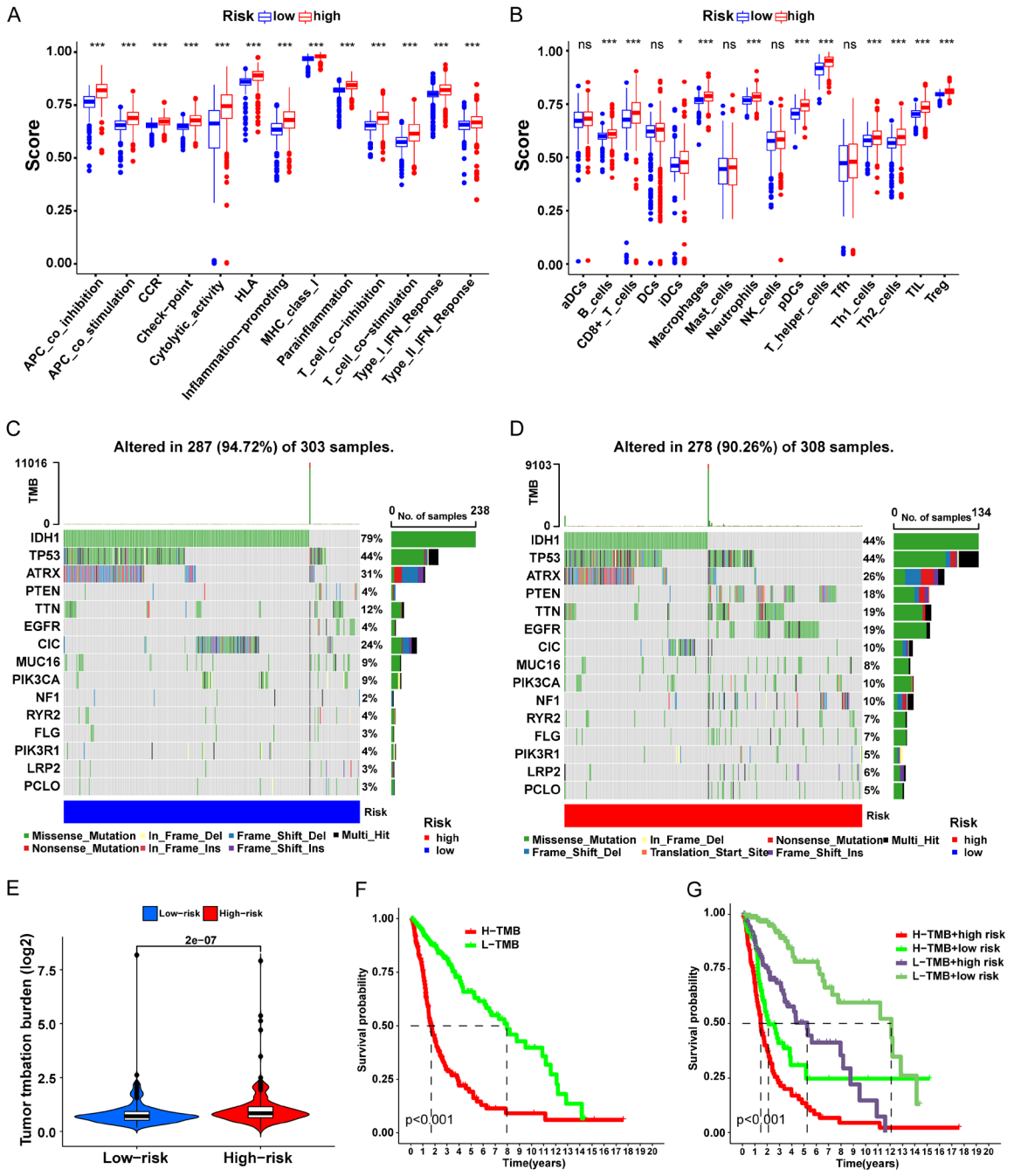

Figure 5. A, B: Heterogeneity of different immune cells and inflammation-related factors in patients with high and low-risk scores were conducted. C, D: Somatic mutation signatures in the immunogenic cell death-related model were shown in a waterfall plot. E: Differences between tumor tmbation burden scores in high and low-risk score groups were analyzed. F: Survival analysis of high and low TMB. G: Survival analysis between different TMB scores and high and low-risk scores.

high ICD subtype. Conversely, the low-risk group exhibited a contrary trend (**Figure 5A**), suggesting a close association between immunosera and cold-resistant phenotypes with the ICD high and low subtypes, respectively.

Diverse somatic mutation patterns were observed between low-risk and high-risk groups (**Figure 5C**, **5D**). While mutations in genes such as TP53, TTN, FAT1, CDKN2A, and MUC16 were prominent, their relative frequencies varied by subtype. The ICD high subtypes exhibited higher mutation rates in IDH1, TP53, ATRX, and TTN, accounting for 79%, 44%, 31%, and 12% of the total, respectively, compared to 44%, 26%, 26%, and 19% in the ICD low subtypes.

Clinical trials and preclinical studies have linked high somatic TMB with improved response, enhanced long-term survival, and sustained therapeutic benefits in patients undergoing immunocheckpoint blockade therapy [29]. We analyzed various TMB risk-scores and found that the low-scoring group had a better prognosis, while the high-scoring group exhibited a higher TMB (**Figure 5E-G**). This suggests that the ICD prediction model could be instrumental in forecasting glioma patients' prognosis and may indicate their response to immunotherapy.

The tumor microenvironmental landscape of different ICD subtypes

Emerging evidence indicates the critical role of ICDs in eliciting specific anti-tumor immune responses. Notably, our findings showed that C2 and C3 subtypes exhibited higher rates of immune cell infiltration compared to the C1 subtype. We then analyzed the TME structure across the three ICD subtypes. Results revealed variation in ESTIMATE immune scores among the subtypes, with the C3 subtype demonstrating higher immune activity than both C2 and C1 subtypes. This suggests that ICD heterogeneity may influence responses to immunotherapy, with C3 subtypes exhibiting stronger immune reactions compared to C1 and C2 subtypes (**Figure 6A-C**). Thus, TME cell differences may be a key factor driving ICD heterogeneity, supporting previous findings that "hot tumors" were tumors that were associated with more T cell infiltration, making the tumors more responsive to immunotherapy, and yielding better therapeutic outcomes [30].

To further explore the relationship between ICD subtypes and immunotherapies, such as PD1/PDL1 inhibitors, we examined variations in immune checkpoint expression across the subtypes. The majority of immunological checkpoints were found to be differentially expressed among ICD subtypes. Notably, C3 subtypes expressed higher levels of most immune checkpoint genes compared to C1 and C2 subtypes (**Figure 6D**). This indicates that ICD heterogeneity could predict the effectiveness of immunotherapy in glioma patients, particularly in those with the C3 subtype.

Tissue validation results

We validated the differences in the expression of BAX, MYD88, and CASP8 in glioma versus normal tissues using Western blotting. The results demonstrated higher expression of BAX, MYD88, and CASP8 in glioma tissues (**Figure 7A**). Notably, the RT-qPCR assay showed similar results (**Figure 7B**). We then looked for immunohistochemical results of BAX, CASP8, and MYD88 in the HPA database. Our immunohistochemical results also indicated significantly higher expression of these genes in glioblastoma (GBM) patient tissues (**Figure 7C-E**). Surprisingly, IHC data from several centers corroborated these findings, showing significantly elevated expression of BAX, CASP8, and MYD88 in glioma tissues (Supplementary Figure 4). These findings align with our previous analyses, confirming that BAX, CASP8, and MYD88 are highly expressed in glioma tissues and may play roles in glioma genesis and progression.

Consensus clustering identified three ICD associated subtypes

Based on their expression, we classified the IRGs into three ICD related subtypes in order to determine the optimum clustering stability at K = 3 (Supplementary Figure 5A, 5B). Of the 631 glioma patients included in the study, 323 were clustered into C1 subtypes, 238 into C2 subtypes, and 70 were pressed into C3 subtypes. Normalized enrichment scores for IRGs across the three subtypes are shown using a heatmap (Supplementary Figure 6). Additionally, we analyzed TME cell infiltration in these ICD subtypes (Supplementary Figure 6). PCA and tSNE analyses revealed that patients in all three groups were distinct and distinguishable from each

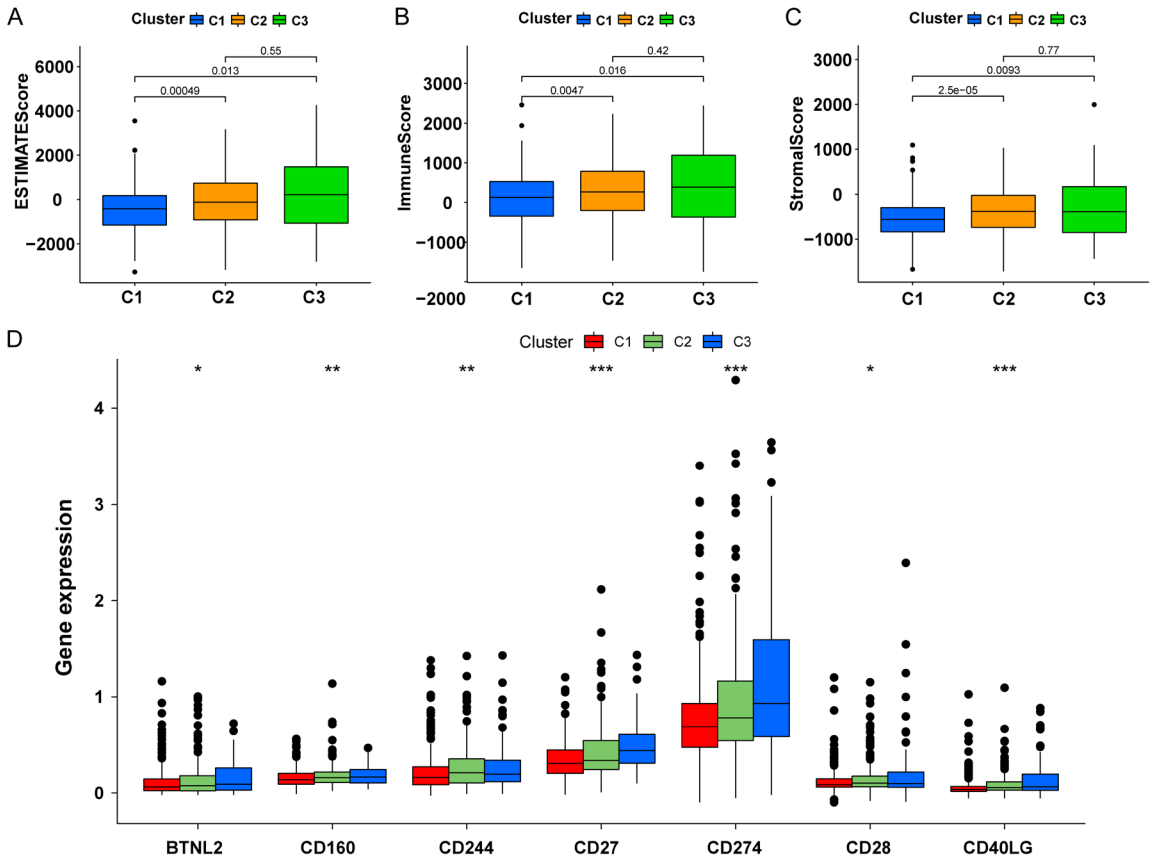

Figure 6. A-C: Differences between stromal score, immune score, and estimate score in three Gene clusters are demonstrated. D: The image shows differences in the expression of immune checkpoint-related genes in the three gene clusters.

other (Supplementary Figure 5C-F). Furthermore, survival analysis of these ICD-based subgroups indicated varying clinical outcomes, with the C1 subtype exhibiting a better prognosis compared to the C2 and C3 subtypes, and the C3 subtype demonstrating the worst prognosis (Supplementary Figure 5G). Sankey diagram further indicated that C1 subtype patients had lower risk scores compared to those in the C3 subtype (Supplementary Figure 5H). These results suggest that our risk model accurately staged glioma patients' prognoses and that the ICD subtypes may have predictive value for clinical interventions, particularly immunotherapy.

Correlation analysis of risk scores and drug sensitivity

The link between risk ratings and glioma treatment medications was analyzed to investigate the effect of ICD-related prediction models on glioma drug treatment responses. A strong correlation was found between risk scores and drug treatment effectiveness (Supplementary Figure 7A-H). This suggests that IRGs might be associated with glioma treatment resistance and could serve as potential targets for glioma drug therapy.

Impact of BAX knockout on GBM progression

To understand the pathophysiological role of BAX in GBM, we used RNA interference to suppress endogenous BAX expression. The efficiency of gene knockout was determined via RT-qPCR. Sequence one exhibited a higher knockout efficiency in U251 cells, while sequence two was more effective in ln229 cells. Accordingly, sequence one was used for U251 cells and sequence two for ln229 cells, facilitating subsequent experiments (**Figure 8A**). The influence of BAX on GBM proliferation was validated using the CCK-8 assay, indicating

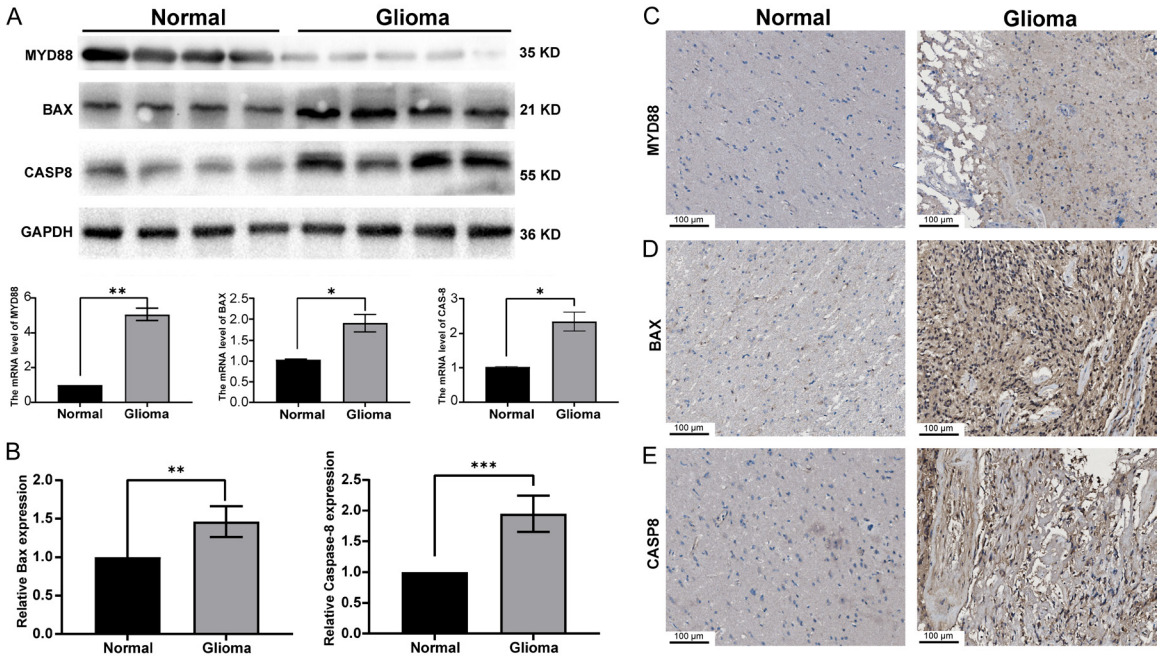

Figure 7. ICD-Related DEGs were highly expressed in glioma tissues. A: WB detection of MYD88, BAX and CASP8 expression in glioma and normal tissues. B: RT-qPCR to detect the expression levels of MYD88, BAX and CASP8 in glioma and normal brain tissues. C-E: Immunohistochemical detection of BAX, CASP8 and MYD88 expression in glioma tissues and normal tissues (Data are means ± SD of at least three independent experiments with Student's t-test or one-way ANOVA (*$P < 0.05$; ns, not significant)).

that the suppression of BAX significantly reduced the in vitro proliferative capacity of both U251 and In229 cell strains (**Figure 8B**). Furthermore, we examined the impact of BAX knockout on the migration and invasion potential of U251 and In229 (**Figure 8C**, **8D**). The results showed that inhibiting BAX markedly reduced migration and invasion potential (**Figure 8E**, **8F**). These findings highlight the crucial role of BAX in promoting GBM cell proliferation, migration, and invasion.

Discussion

Central nervous system tumors are the most prevalent solid tumors in children. with gliomas being the most prevalent malignant type [31]. Characterized by high-grade disease, high recurrence rates, and mortality, gliomas account for 50% of these malignancies [32]. The traditional classification of gliomas, based solely on histology, is insufficient in the era of advanced genomics and molecular diagnostics. Recent advancements have significantly transformed the classification of pediatric gliomas, shifting from morphological to molecular stratification. This molecular-focused approach offers a more reliable categorization of gliomas and opens up new avenues for treatment strategies. Notably, emerging molecular biomarkers have been recognized, including chromosome 1p/19q co-deletion and IDH mutation, incorporated into the stratified glioma classification in the 2016 WHO guidelines for the first time [33]. Despite advances in immunotherapy improving outcomes in certain cancers, optimal management of gliomas remains a significant challenge [34].

Immunogenic cell death is a unique form of regulatory cell death that can initiate a comprehensive antigen-specific adaptive immune response through the release of danger signals or DAMPs [10, 14, 35]. Novel immunotherapeutic strategies combined with immunogenic therapy offer promising prospects for parent therapy [13, 36-38]. Identifying ICD-related biomarkers that distinguish glioma patients' responsiveness to immunotherapy is crucial. To date, few studies have explored the role of immunogenic cell death in glioma classification. Our study extensively examined the relationship between IRGs and glioma, identifying three distinct glioma subgroups based on prognostic

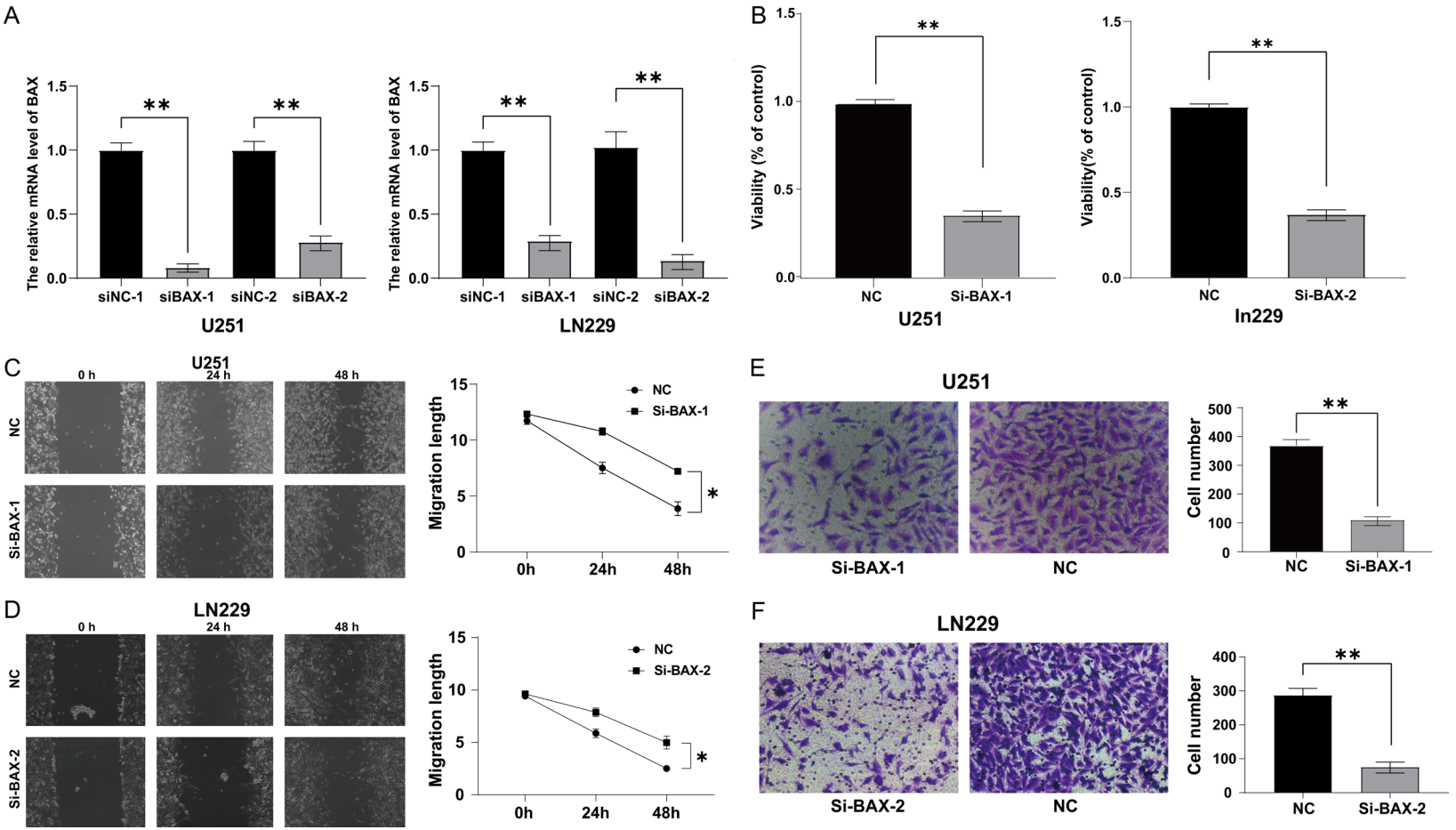

Figure 8. A: RT-qPCR was performed to determine the knockdown efficiency of sequence 1 in U251 cells and sequence 2 in LN229 cells. B: CCK-8 detects the effect of knockdown on the proliferation of U251 and LN229. C, D: Images of Si-BAX U251 and LN229 exposed at different times (0, 24 and 48 h) compared to the control group. Distance curves of Si-BAX U251 and LN229 groups from the control group (Statistical analysis was performed using two-way ANOVA and Sidack post hoc tests. Values are means ± s.e.m. (n = 4)). E, F: Transwell assay to analyze the migration and invasion ability of si-BAX and normal control U251 and LN229 cells.

genes associated with ICD and constructing an immunological spectrum for each group. We also detailed the molecular and clinical characteristics of each subgroup/risk group, providing novel perspectives into pediatric glioma classification and malignancy progression.

In this study, we initially described the expression of ICD-related prognostic genes in gliomas, constructing a signature comprising three key genes: BCL2 Associated X (BAX), Caspase 8 (CASP8), and Myeloid Differentiation Primary Response Gene (88) (MyD88). BAX is a central regulator of cell death, an indispensable pathway for mitochondrial dysfunction, and a core pro-apoptotic member of the Bcl-2 protein family that controls apoptosis in both standard and cancer cells. Dysfunctional apoptosis can lead to cancer cell resistance to treatment and promote tumorigenesis. Several recent studies had suggested that the aberrant expression of BAX might be associated with chemoresistance in ovarian, colorectal, lung, and melanoma cancers [39-43]. BAX activators could promote pro-apoptotic activity, potentially overcoming drug resistance, serving as an alternative to enhanced BAX expression, increasing apoptotic stimulation, and reducing tumor expansion [44]. Several direct BAX activators have been identified with specificity advantages and potential to overcome resistance to chemotherapy and radiotherapy. These properties are pivotal in cancer treatment. Further studies on these new drug candidate are needed to bring them to the clinic as a new treatment for cancer [45].

CASP8, an apical cysteine-aspartic acid protease, induces lysosome-associated cell death in cancer cells [46]. It classically triggers an external pathway of apoptosis in response to activation of cell surface death receptors (DR), such as FAS, TRAIL-R, and TNF-R. In addition to its role in triggering death receptor-mediated apoptosis, caspase-8 is thought to be associated with the development of denuded apoptosis, autophagy, and cellular scorching [47]. Besides its role in apoptosis, caspase-8 has been implicated in non-apoptotic functions, such as promoting NF-κB activation, autophagy regulation and endosome transport change. Therefore, dependent on specific cellular background, caspase-8 may enhance or inhibit malignant transformation of tumors. The expression pattern of caspase-8 displays notable heterogeneity across different tumor types. Therapy aimed at increasing caspase-8 expression has been developed, but its efficacy across all cases remains uncertain [48].

MyD88 acts as a typical bridging element in the downstream inflammatory signaling pathways for members of the Toll-like receptor (TLR) and interleukin-1 (IL-1) receptor families. Recent studies have demonstrated that MyD88 promotes proliferation and metastasis in various cancers, including pancreatic, colorectal, lymphoma, and breast cancers, by mediating inflammatory responses in the TME [49-53]. In the present study, we found that most glioma patients exhibited high expression of these ICD genes, which are associated with glioma prognosis. KEGG analysis revealed that these IRGs are involved in essential pathways related to tumor immunity, such as antigen processing and presentation, macrophage differentiation, and positive regulation of IL-1. These results suggest that a signature constructed from these three ICD prognosis-associated genes is important to glioma immunotherapy.

To further explore the utility of our ICD-related signature in the stratification of glioma patients, patient samples were scored using our ICD-related signature and were successfully classified into high- and low-risk groups based on median risk scores. This classification utilized ROC curves, PCA, stratified analysis, multivariate regression analysis, and univariate regression analysis, alongside the TCGA training cohort for survival analysis. Our findings indicated that well-known genetic traits serve as reliable indicators for prognosis prediction. Moreover, the CGGA external validation cohort presented comparable results, reinforcing the validity of our approach.

A well-known technique is sample classification based on parameters of preset gene expression [54]. This method was used in the current investigation to divide glioma patients into three subgroups. This analysis revealed significant heterogeneity in the expression of these IRGs among the subtypes. Additionally, there was a strong correlation between these regulators and other survival hazards. PCA analysis suggested a possible distinction of these three subtypes among glioma patients, with the C3

subtype demonstrating the worst prognosis among independent patients.

Immune cells use cell migration to carry out their immunosurveillance role. The glioma TME is incredibly intricate. Myeloid cells associated with gliomas are crucial in increasing the virulence of glioma cells [55]. We used ssGSEA and CIBERSORT to investigate the brain immune microenvironment in glioma patients. According to correlation heat maps, patients with high risk scores had considerably greater numbers of B-cell plasma, CD8 T cells, macrophages M1 and M2, activated myeloid dendritic cells, and regulatory T cells. Conversely, the low-risk group exhibited reduced numbers of these immune cells. Previous evidence suggests that the malignant biological behavior of glioma cells is influenced by the polarization of M2 macrophages in the TME [56]. Furthermore, regulatory T cell infiltration has been closely linked to poor prognosis [56]. Consistent with earlier studies, our results demonstrated increased infiltration of macrophages, myeloid dendritic cells, and regulatory T cells in patients with higher risk scores.

These results support the idea that patient characteristics are intimately linked to immune cell infiltration, corroborating earlier studies. To further differentiate between glioma patient groups that responded better to immunotherapy, we subdivided the study's glioblastoma patients into three distinct subgroups. Further genotyping demonstrated that the three distinct subgroups differed in terms of ESTIMATE score, immune score, and stromal score, with subtype C3 having the highest ESTIMATE score, immunological score, and stromal score, whereas subtype C1 had the lowest. Tumor purity had a low group correlation. These findings implied that patients with high-risk gliomas had more immune cell infiltration in the tumor immunological microenvironment. Our results align with previous research indicating a correlation between tumor grade and increased immune cell infiltration. Surprisingly, the current study also discovered high TMB scores, resistant cell infiltration rates, stronger immune checkpoint gene expression, and a more potent immunotherapy response in the C3 cohort than in the other two subgroups. The C1 subtype is sometimes referred to as the immunologically 'cold' phenotype and the C3 subtype as the 'hot' phenotype. These findings imply that our ICD-related genotyping could predict immunotherapeutic responses in glioma patients, potentially opening new therapeutic avenues.

In conclusion, our research highlights the connection between ICD subtypes and changes in the immunological tumor microenvironment in glioma patients. This insight could facilitate the selection of immunotherapy-based treatments for glioma patients. Additionally, we developed and validated ICD-related predictive features useful for forecasting overall survival (OS) in glioma patients.

Conclusion

Based on our data, we established ICD-associated features to stratify prognosis and predict responsiveness to immune checkpoint inhibitor therapy, identifying three ICD-associated subgroups in gliomas. Our findings offer a new perspective on glioma classification and underscore the role of ICD-related prognostic genetic characteristics in glioma heterogeneity. This study also revealed that different risk subgroups differed in immune cell infiltration and immune checkpoint-related gene expression. These results suggest a promising approach to determine a patient's risk prediction for glioma and potentially create more effective management and treatment strategies for those affected by the disease.

Acknowledgements

The authors of this paper are very grateful for the help provided by the following platforms and people: TCGA, CGGA and HPA for providing important data; Harbin Medical University provided the experimental platform; Kan Wang responsible for the experimental validation part.

Disclosure of conflict of interest

None.

Abbreviations

ICD, Immunogenic cell death; CNS, central nervous system; IRGs, ICD-related genes; LASSO, Least Absolute Shrinkage and Selection Operator; ICD-related-DEGs, immune cell death-

related-differential genes; RT-qPCR, quantitative reverse transcription polymerase chain reaction; WB, Western blot; IHC, immunohistochemistry; TCGA, The Cancer Genome Atlas; CGGA, Chinese Glioma Genome Atlas; TCGA-LGG, TCGA-Lower-grade glioma; TCGA-GBM, TCGA-Glioblastoma; DEGs, differentially expressed genes; GO, Gene Ontology; KEGG, Kyoto Encyclopedia of Genes and Genomes; TME, Tumour Microenvironment; ssGSEA, single sample gene set enrichment analysis; SNP, single nucleotide polymorphism; CNV, copy number variation; TMB, tumor mutational burden; ROC, receiver operating characteristic; IC50, half maximal inhibitory concentration; GDSC, Genomics of Drug Sensitivity in Cancer; AUC, area under the curve; BPs, biological processes; CCs, Cellular components; MHC, major histocompatibility complex; MFs, molecular functions; HLA, human leukocyte antigen; BAX, BCL2 Associated X; CASP8, Caspase8; MyD88, Myeloid Differentiation Primary Response Gene (88); TLR, Toll-like receptor; IL-1, interleukin-1; CCK-8, Cell Counting Kit-8.

Address correspondence to: Zhiteng Yan, Longgang District Maternity and Child Healthcare Hospital of Shenzhen City (Longgang Maternity and Child Institute of Shantou University Medical College), Shenzhen, Guangdong, China. E-mail: yanzhiteng-2023@163.com

References

[1] Filbin MG and Sturm D. Gliomas in children. Semin Neurol 2018; 38: 121-130.

[2] Sturm D, Pfister SM and Jones DTW. Pediatric gliomas: current concepts on diagnosis, biology, and clinical management. J Clin Oncol 2017; 35: 2370-2377.

[3] Wang TJC and Mehta MP. Low-grade glioma radiotherapy treatment and trials. Neurosurg Clin N Am 2019; 30: 111-118.

[4] Delgado-López PD, Corrales-García EM, Martino J, Lastra-Aras E and Dueñas-Polo MT. Diffuse low-grade glioma: a review on the new molecular classification, natural history and current management strategies. Clin Transl Oncol 2017; 19: 931-944.

[5] Esparragosa I, Díez-Valle R, Tejada S and Gállego Pérez-Larraya J. Management of diffuse glioma. Presse Med 2018; 47: e199-e212.

[6] Li S and Ding X. TRPC channels and glioma. Adv Exp Med Biol 2017; 976: 157-165.

[7] Ostrom QT, Bauchet L, Davis FG, Deltour I, Fisher JL, Langer CE, Pekmezci M, Schwartzbaum JA, Turner MC, Walsh KM, Wrensch MR and Barnholtz-Sloan JS. The epidemiology of glioma in adults: a "state of the science" review. Neuro Oncol 2014; 16: 896-913.

[8] Gao YF, Liu JY, Mao XY, He ZW, Zhu T, Wang ZB, Li X, Yin JY, Zhang W, Zhou HH and Liu ZQ. LncRNA FOXD1-AS1 acts as a potential oncogenic biomarker in glioma. CNS Neurosci Ther 2020; 26: 66-75.

[9] Orukari IE, Siegel JS, Warrington NM, Baxter GA, Bauer AQ, Shimony JS, Rubin JB and Culver JP. Altered hemodynamics contribute to local but not remote functional connectivity disruption due to glioma growth. J Cereb Blood Flow Metab 2020; 40: 100-115.

[10] Galluzzi L, Vitale I, Warren S, Adjemian S, Agostinis P, Martinez AB, Chan TA, Coukos G, Demaria S, Deutsch E, Draganov D, Edelson RL, Formenti SC, Fucikova J, Gabriele L, Gaipl US, Gameiro SR, Garg AD, Golden E, Han J, Harrington KJ, Hemminki A, Hodge JW, Hossain DMS, Illidge T, Karin M, Kaufman HL, Kepp O, Kroemer G, Lasarte JJ, Loi S, Lotze MT, Manic G, Merghoub T, Melcher AA, Mossman KL, Prosper F, Rekdal Ø, Rescigno M, Riganti C, Sistigu A, Smyth MJ, Spisek R, Stagg J, Strauss BE, Tang D, Tatsuno K, van Gool SW, Vandenabeele P, Yamazaki T, Zamarin D, Zitvogel L, Cesano A and Marincola FM. Consensus guidelines for the definition, detection and interpretation of immunogenic cell death. J Immunother Cancer 2020; 8: e000337.

[11] Kroemer G, Galassi C, Zitvogel L and Galluzzi L. Immunogenic cell stress and death. Nat Immunol 2022; 23: 487-500.

[12] Fucikova J, Kepp O, Kasikova L, Petroni G, Yamazaki T, Liu P, Zhao L, Spisek R, Kroemer G and Galluzzi L. Detection of immunogenic cell death and its relevance for cancer therapy. Cell Death Dis 2020; 11: 1013.

[13] Kroemer G, Galluzzi L, Kepp O and Zitvogel L. Immunogenic cell death in cancer therapy. Annu Rev Immunol 2013; 31: 51-72.

[14] Krysko DV, Garg AD, Kaczmarek A, Krysko O, Agostinis P and Vandenabeele P. Immunogenic cell death and DAMPs in cancer therapy. Nat Rev Cancer 2012; 12: 860-875.

[15] Ahmed A and Tait SWG. Targeting immunogenic cell death in cancer. Mol Oncol 2020; 14: 2994-3006.

[16] Tsvetkov P, Coy S, Petrova B, Dreishpoon M, Verma A, Abdusamad M, Rossen J, Joesch-Cohen L, Humeidi R, Spangler RD, Eaton JK, Frenkel E, Kocak M, Corsello SM, Lutsenko S, Kanarek N, Santagata S and Golub TR. Copper induces cell death by targeting lipoylated TCA cycle proteins. Science 2022; 375: 1254-1261.

[17] von Mering C, Jensen LJ, Snel B, Hooper SD, Krupp M, Foglierini M, Jouffre N, Huynen MA and Bork P. STRING: known and predicted protein-protein associations, integrated and transferred across organisms. Nucleic Acids Res 2005; 33: D433-D437.
[18] Yu G, Wang LG, Han Y and He QY. clusterProfiler: an R package for comparing biological themes among gene clusters. OMICS 2012; 16: 284-287.
[19] Engebretsen S and Bohlin J. Statistical predictions with glmnet. Clin Epigenetics 2019; 11: 123.
[20] Wilkerson MD and Hayes DN. ConsensusClusterPlus: a class discovery tool with confidence assessments and item tracking. Bioinformatics 2010; 26: 1572-1573.
[21] Newman AM, Liu CL, Green MR, Gentles AJ, Feng W, Xu Y, Hoang CD, Diehn M and Alizadeh AA. Robust enumeration of cell subsets from tissue expression profiles. Nat Methods 2015; 12: 453-457.
[22] Rooney MS, Shukla SA, Wu CJ, Getz G and Hacohen N. Molecular and genetic properties of tumors associated with local immune cytolytic activity. Cell 2015; 160: 48-61.
[23] Yang Z, Liang X, Fu Y, Liu Y, Zheng L, Liu F, Li T, Yin X, Qiao X and Xu X. Identification of AUNIP as a candidate diagnostic and prognostic biomarker for oral squamous cell carcinoma. EBioMedicine 2019; 47: 44-57.
[24] Yoshihara K, Shahmoradgoli M, Martínez E, Vegesna R, Kim H, Torres-Garcia W, Treviño V, Shen H, Laird PW, Levine DA, Carter SL, Getz G, Stemke-Hale K, Mills GB and Verhaak RG. Inferring tumour purity and stromal and immune cell admixture from expression data. Nat Commun 2013; 4: 2612.
[25] Mayakonda A, Lin DC, Assenov Y, Plass C and Koeffler HP. Maftools: efficient and comprehensive analysis of somatic variants in cancer. Genome Res 2018; 28: 1747-1756.
[26] Iasonos A, Schrag D, Raj GV and Panageas KS. How to build and interpret a nomogram for cancer prognosis. J Clin Oncol 2008; 26: 1364-1370.
[27] Geeleher P, Cox N and Huang RS. pRRophetic: an R package for prediction of clinical chemotherapeutic response from tumor gene expression levels. PLoS One 2014; 9: e107468.
[28] Uhlén M, Fagerberg L, Hallström BM, Lindskog C, Oksvold P, Mardinoglu A, Sivertsson Å, Kampf C, Sjöstedt E, Asplund A, Olsson I, Edlund K, Lundberg E, Navani S, Szigyarto CA, Odeberg J, Djureinovic D, Takanen JO, Hober S, Alm T, Edqvist PH, Berling H, Tegel H, Mulder J, Rockberg J, Nilsson P, Schwenk JM, Hamsten M, von Feilitzen K, Forsberg M, Persson L, Johansson F, Zwahlen M, von Heijne G, Nielsen J and Pontén F. Proteomics. Tissue-based map of the human proteome. Science 2015; 347: 1260419.
[29] Zhang B, Wu Q, Li B, Wang D, Wang L and Zhou YL. m(6)A regulator-mediated methylation modification patterns and tumor microenvironment infiltration characterization in gastric cancer. Mol Cancer 2020; 19: 53.
[30] Li J, Byrne KT, Yan F, Yamazoe T, Chen Z, Baslan T, Richman LP, Lin JH, Sun YH, Rech AJ, Balli D, Hay CA, Sela Y, Merrell AJ, Liudahl SM, Gordon N, Norgard RJ, Yuan S, Yu S, Chao T, Ye S, Eisinger-Mathason TSK, Faryabi RB, Tobias JW, Lowe SW, Coussens LM, Wherry EJ, Vonderheide RH and Stanger BZ. Tumor cell-intrinsic factors underlie heterogeneity of immune cell infiltration and response to immunotherapy. Immunity 2018; 49: 178-193, e177.
[31] Chalil A and Ramaswamy V. Low grade gliomas in children. J Child Neurol 2016; 31: 517-522.
[32] Qi Y, Liu B, Sun Q, Xiong X and Chen Q. Immune checkpoint targeted therapy in glioma: status and hopes. Front Immunol 2020; 11: 578877.
[33] Louis DN, Perry A, Reifenberger G, von Deimling A, Figarella-Branger D, Cavenee WK, Ohgaki H, Wiestler OD, Kleihues P and Ellison DW. The 2016 World Health Organization classification of tumors of the central nervous system: a summary. Acta Neuropathol 2016; 131: 803-820.
[34] Boussiotis VA and Charest A. Immunotherapies for malignant glioma. Oncogene 2018; 37: 1121-1141.
[35] Serrano-Del Valle A, Anel A, Naval J and Marzo I. Immunogenic cell death and immunotherapy of multiple myeloma. Front Cell Dev Biol 2019; 7: 50.
[36] Duan X, Chan C and Lin W. Nanoparticle-mediated immunogenic cell death enables and potentiates cancer immunotherapy. Angew Chem Int Ed Engl 2019; 58: 670-680.
[37] Li Y, Zhang H, Li Q, Zou P, Huang X, Wu C and Tan L. CDK12/13 inhibition induces immunogenic cell death and enhances anti-PD-1 anticancer activity in breast cancer. Cancer Lett 2020; 495: 12-21.
[38] Yang W, Zhang F, Deng H, Lin L, Wang S, Kang F, Yu G, Lau J, Tian R, Zhang M, Wang Z, He L, Ma Y, Niu G, Hu S and Chen X. Smart nanovesicle-mediated immunogenic cell death through tumor microenvironment modulation for effective photodynamic immunotherapy. ACS Nano 2020; 14: 620-631.
[39] Fresquet V, Rieger M, Carolis C, García-Barchino MJ and Martinez-Climent JA. Acquired mutations in BCL2 family proteins conferring resistance to the BH3 mimetic ABT-199 in lymphoma. Blood 2014; 123: 4111-4119.

[40] Igney FH and Krammer PH. Death and anti-death: tumour resistance to apoptosis. Nat Rev Cancer 2002; 2: 277-288.
[41] Manoochehri M, Karbasi A, Bandehpour M and Kazemi B. Down-regulation of BAX gene during carcinogenesis and acquisition of resistance to 5-FU in colorectal cancer. Pathol Oncol Res 2014; 20: 301-307.
[42] Perego P, Giarola M, Righetti SC, Supino R, Caserini C, Delia D, Pierotti MA, Miyashita T, Reed JC and Zunino F. Association between cisplatin resistance and mutation of p53 gene and reduced bax expression in ovarian carcinoma cell systems. Cancer Res 1996; 56: 556-562.
[43] Quast SA, Berger A, Plötz M and Eberle J. Sensitization of melanoma cells for TRAIL-induced apoptosis by activation of mitochondrial pathways via Bax. Eur J Cell Biol 2014; 93: 42-48.
[44] Bargou RC, Wagener C, Bommert K, Mapara MY, Daniel PT, Arnold W, Dietel M, Guski H, Feller A, Royer HD and Dörken B. Overexpression of the death-promoting gene bax-alpha which is downregulated in breast cancer restores sensitivity to different apoptotic stimuli and reduces tumor growth in SCID mice. J Clin Invest 1996; 97: 2651-2659.
[45] Liu Z, Ding Y, Ye N, Wild C, Chen H and Zhou J. Direct activation of bax protein for cancer therapy. Med Res Rev 2016; 36: 313-341.
[46] Zhong B, Liu M, Bai C, Ruan Y, Wang Y, Qiu L, Hong Y, Wang X, Li L and Li B. Caspase-8 induces lysosome-associated cell death in cancer cells. Mol Ther 2020; 28: 1078-1091.
[47] Mandal R, Barrón JC, Kostova I, Becker S and Strebhardt K. Caspase-8: the double-edged sword. Biochim Biophys Acta Rev Cancer 2020; 1873: 188357.
[48] Stupack DG. Caspase-8 as a therapeutic target in cancer. Cancer Lett 2013; 332: 133-140.
[49] Wang L, Yu K, Zhang X and Yu S. Dual functional roles of the MyD88 signaling in colorectal cancer development. Biomed Pharmacother 2018; 107: 177-184.
[50] Wu K, Zhang H, Fu Y, Zhu Y, Kong L, Chen L, Zhao F, Yu L and Chen X. TLR4/MyD88 signaling determines the metastatic potential of breast cancer cells. Mol Med Rep 2018; 18: 3411-3420.
[51] Yu X, Li W, Deng Q, Li L, Hsi ED, Young KH, Zhang M and Li Y. MYD88 L265P mutation in lymphoid malignancies. Cancer Res 2018; 78: 2457-2462.
[52] Zhu G, Cheng Z, Huang Y, Zheng W, Yang S, Lin C and Ye J. MyD88 mediates colorectal cancer cell proliferation, migration and invasion via NF-κB/AP-1 signaling pathway. Int J Mol Med 2020; 45: 131-140.
[53] Zhu X, Burfeind KG, Michaelis KA, Braun TP, Olson B, Pelz KR, Morgan TK and Marks DL. MyD88 signalling is critical in the development of pancreatic cancer cachexia. J Cachexia Sarcopenia Muscle 2019; 10: 378-390.
[54] Cristescu R, Lee J, Nebozhyn M, Kim KM, Ting JC, Wong SS, Liu J, Yue YG, Wang J, Yu K, Ye XS, Do IG, Liu S, Gong L, Fu J, Jin JG, Choi MG, Sohn TS, Lee JH, Bae JM, Kim ST, Park SH, Sohn I, Jung SH, Tan P, Chen R, Hardwick J, Kang WK, Ayers M, Hongyue D, Reinhard C, Loboda A, Kim S and Aggarwal A. Molecular analysis of gastric cancer identifies subtypes associated with distinct clinical outcomes. Nat Med 2015; 21: 449-456.
[55] Glass R and Synowitz M. CNS macrophages and peripheral myeloid cells in brain tumours. Acta Neuropathol 2014; 128: 347-362.
[56] Qian M, Wang S, Guo X, Wang J, Zhang Z, Qiu W, Gao X, Chen Z, Xu J, Zhao R, Xue H and Li G. Hypoxic glioma-derived exosomes deliver microRNA-1246 to induce M2 macrophage polarization by targeting TERF2IP via the STAT3 and NF-κB pathways. Oncogene 2020; 39: 428-442.

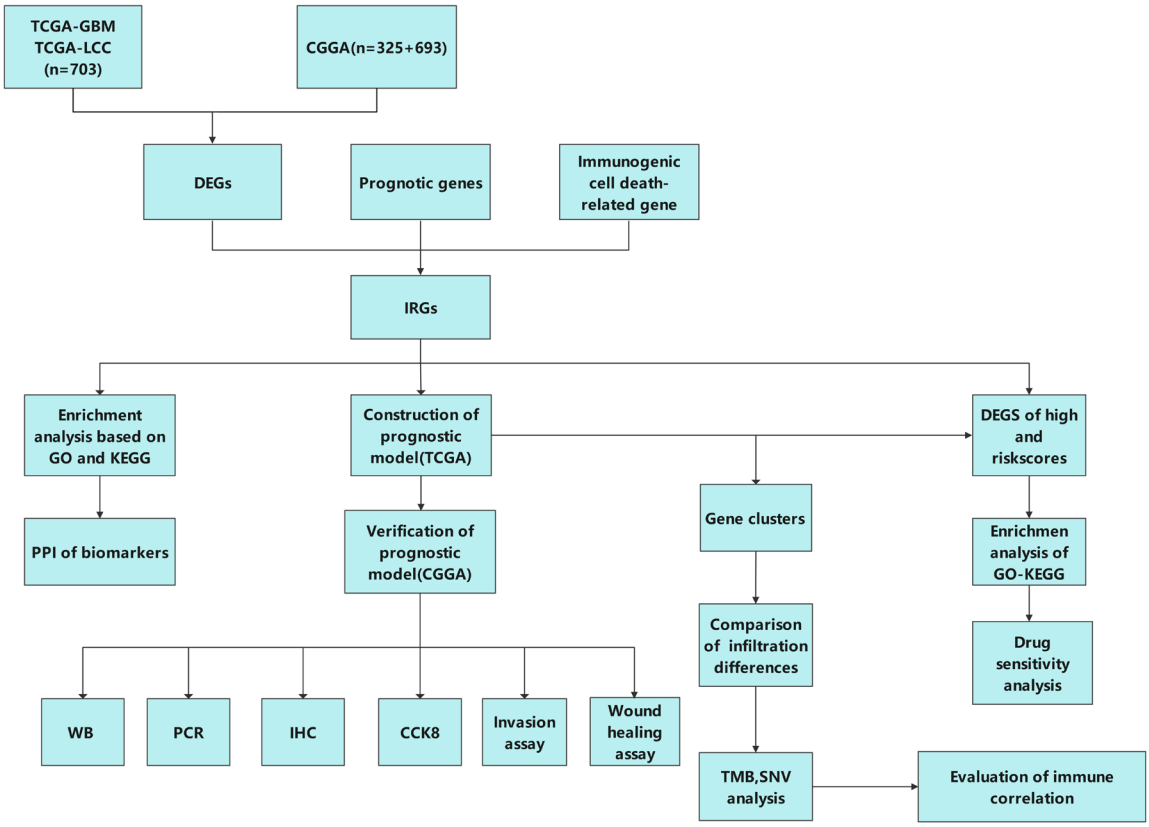

Supplementary Figure 1. The flow chart of this study.

Supplementary Table 1. The clinical characteristics of patients in the TCGA dataset

Variable	Number of samples
Age at diagnosis	
< 65/≥ 65	873/241
Gender	
Male/Female/NA	651/460/3
Grade	
G2/G3/NA	249/265/600

Supplementary Table 2. The clinical characteristics of patients in the CGGA dataset

Variable	Number of samples
Age at diagnosis	
< 65/≥ 65	972/46
Gender	
Male/Female	601/417
Grade	
II/III/IV/NA	291/334/388/5

Supplementary Table 3. The list of Primer sequence (BAX, CASP8 and MYD88)

Gene	
BAX-F	AGCGACTGATGTCCCTGTCTCC
BAX-R	AGATGGTGAGTGAGGCGGTGAG
CASP8-F	GGAGCTGCTCTTCCGAATTA
CASP8-R	CATGACCCTGTAGGCAGAAA
MYD88-F	ACTTGGAGATCCGGCAACT
MYD88-R	ATCCGGCGGCACCAATG

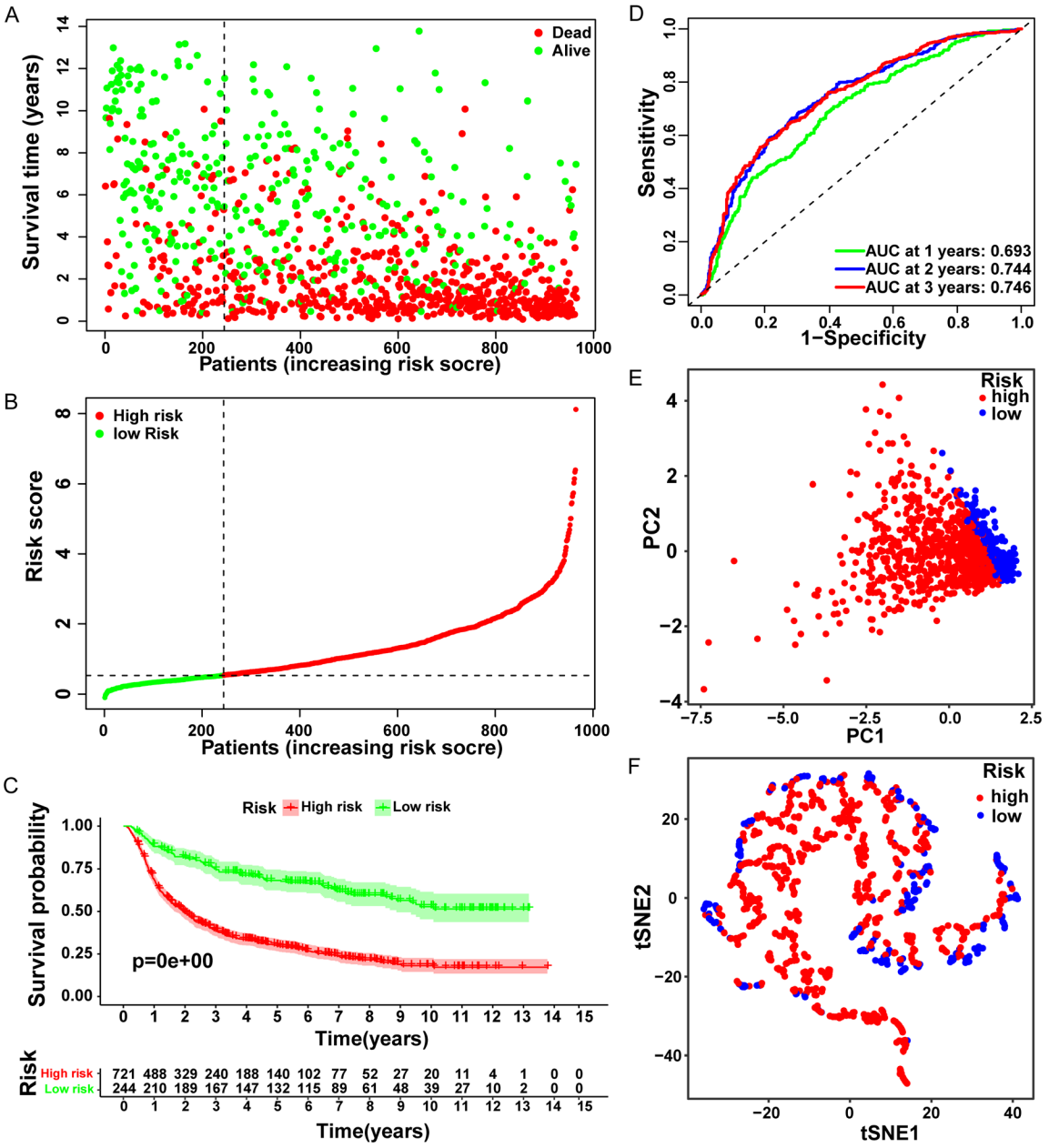

Supplementary Figure 2. Validation of the ICD-associated risk model prediction results in the CGGA dataset. A: Risk score for each patient. B: Survival outcomes for each patient. C: Kaplan-Meier curves are based on the survival of high- and low-risk patients. D: The 1-year, 2-year, and 3-year ROC curves derived from the optimized model construction showed that all AUC values were higher than 0.65. E: PCA results showed that the transcript expression of the two isoforms was significantly different. F: The results of tSNE similarly showed that the transcriptional expression of these two genes was quite different. There is a good distinction between the isoforms of the genes.

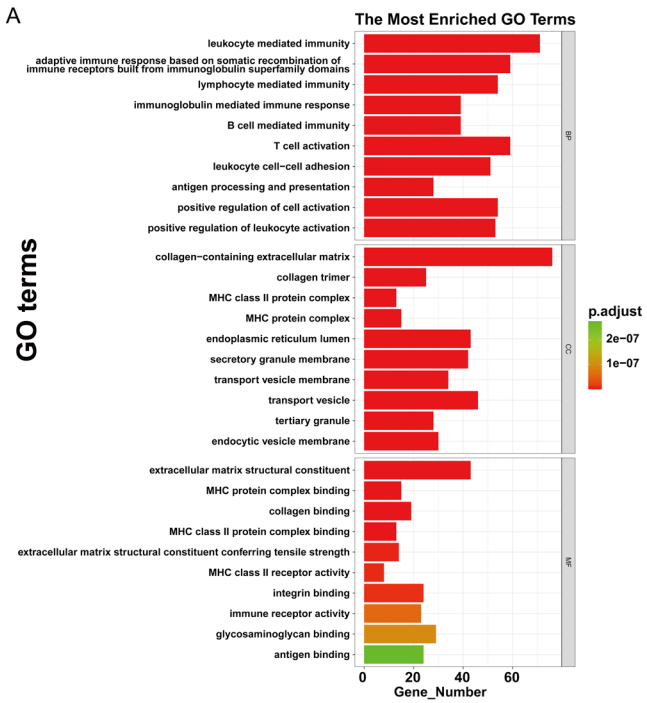
A
The Most Enriched GO Terms
GO terms
leukocyte mediated immunity
adaptive immune response based on somatic recombination of immune receptors built from immunoglobulin superfamily domains
lymphocyte mediated immunity
immunoglobulin mediated immune response
B cell mediated immunity
T cell activation
leukocyte cell−cell adhesion
antigen processing and presentation
positive regulation of cell activation
positive regulation of leukocyte activation
collagen−containing extracellular matrix
collagen trimer
MHC class II protein complex
MHC protein complex
endoplasmic reticulum lumen
secretory granule membrane
transport vesicle membrane
transport vesicle
tertiary granule
endocytic vesicle membrane
extracellular matrix structural constituent
MHC protein complex binding
collagen binding
MHC class II protein complex binding
extracellular matrix structural constituent conferring tensile strength
MHC class II receptor activity
integrin binding
immune receptor activity
glycosaminoglycan binding
antigen binding
BP
CC
MF
p.adjust
2e−07
1e−07
0
20
40
60
Gene_Number

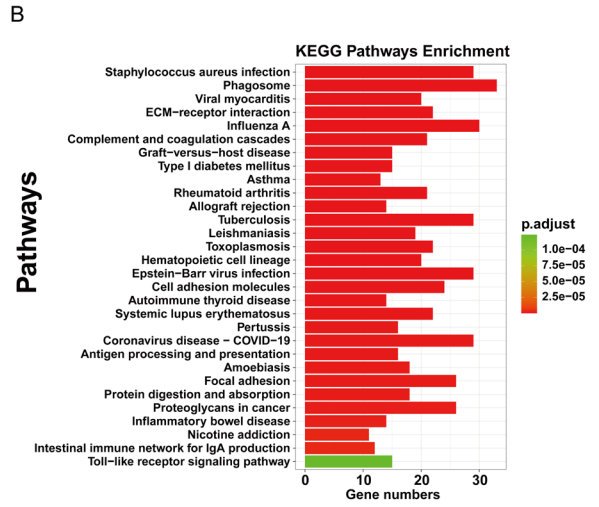
B
KEGG Pathways Enrichment
Pathways
Staphylococcus aureus infection
Phagosome
Viral myocarditis
ECM−receptor interaction
Influenza A
Complement and coagulation cascades
Graft−versus−host disease
Type I diabetes mellitus
Asthma
Rheumatoid arthritis
Allograft rejection
Tuberculosis
Leishmaniasis
Toxoplasmosis
Hematopoietic cell lineage
Epstein−Barr virus infection
Cell adhesion molecules
Autoimmune thyroid disease
Systemic lupus erythematosus
Pertussis
Coronavirus disease − COVID−19
Antigen processing and presentation
Amoebiasis
Focal adhesion
Protein digestion and absorption
Proteoglycans in cancer
Inflammatory bowel disease
Nicotine addiction
Intestinal immune network for IgA production
Toll−like receptor signaling pathway
p.adjust
1.0e−04
7.5e−05
5.0e−05
2.5e−05
0
10
20
30
Gene numbers

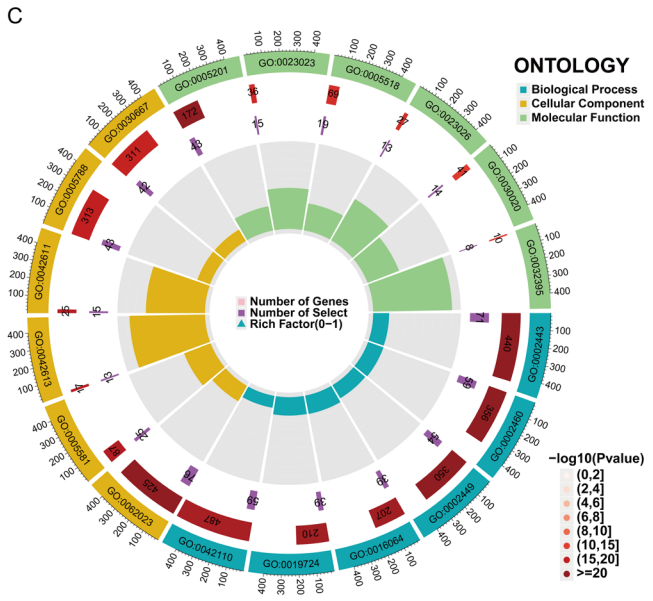
C
ONTOLOGY
Biological Process
Cellular Component
Molecular Function
Number of Genes
Number of Select
Rich Factor(0−1)
−log10(Pvalue)
(0,2]
(2,4]
(4,6]
(6,8]
(8,10]
(10,15]
(15,20]
>=20

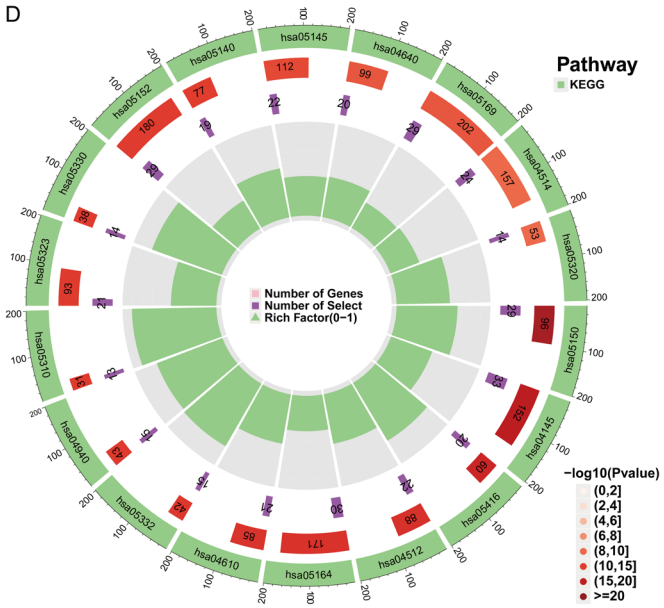
D
Pathway
KEGG
Number of Genes
Number of Select
Rich Factor(0−1)
−log10(Pvalue)
(0,2]
(2,4]
(4,6]
(6,8]
(8,10]
(10,15]
(15,20]
>=20

Supplementary Figure 3. Functional analysis of immunogenic cell death-related genes was conducted. A and C: These images show the enrichment analysis of T cell proliferation-associated regulators BP, CC, and MF. B and D: These images show the enrichment analysis of the KEGG pathway, respectively.

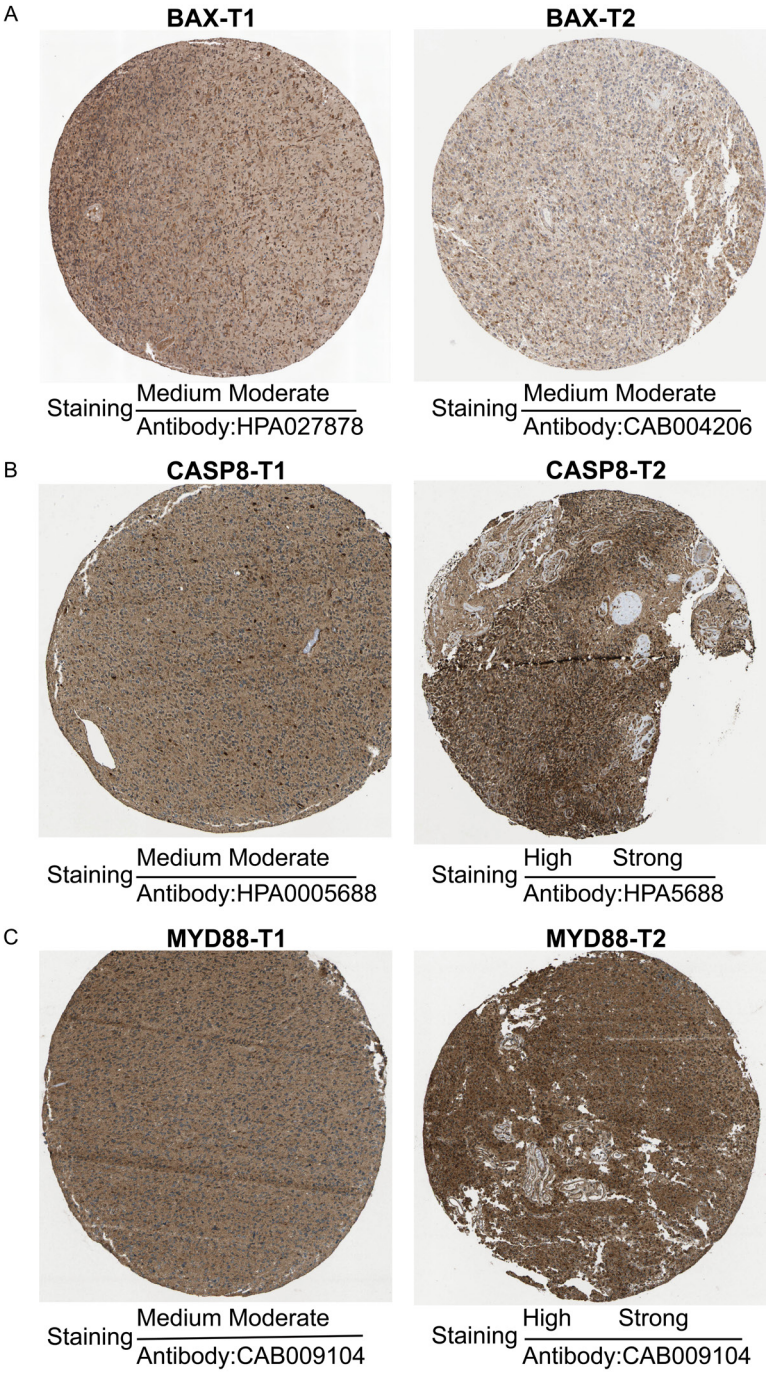

Supplementary Figure 4. Representative immunohistochemical images of (A) BAX, (B) CASP8 and (C) MYD88 in glioma and normal brain tissue from the HPA database. Glioma; HPA, Human Protein Atlas.

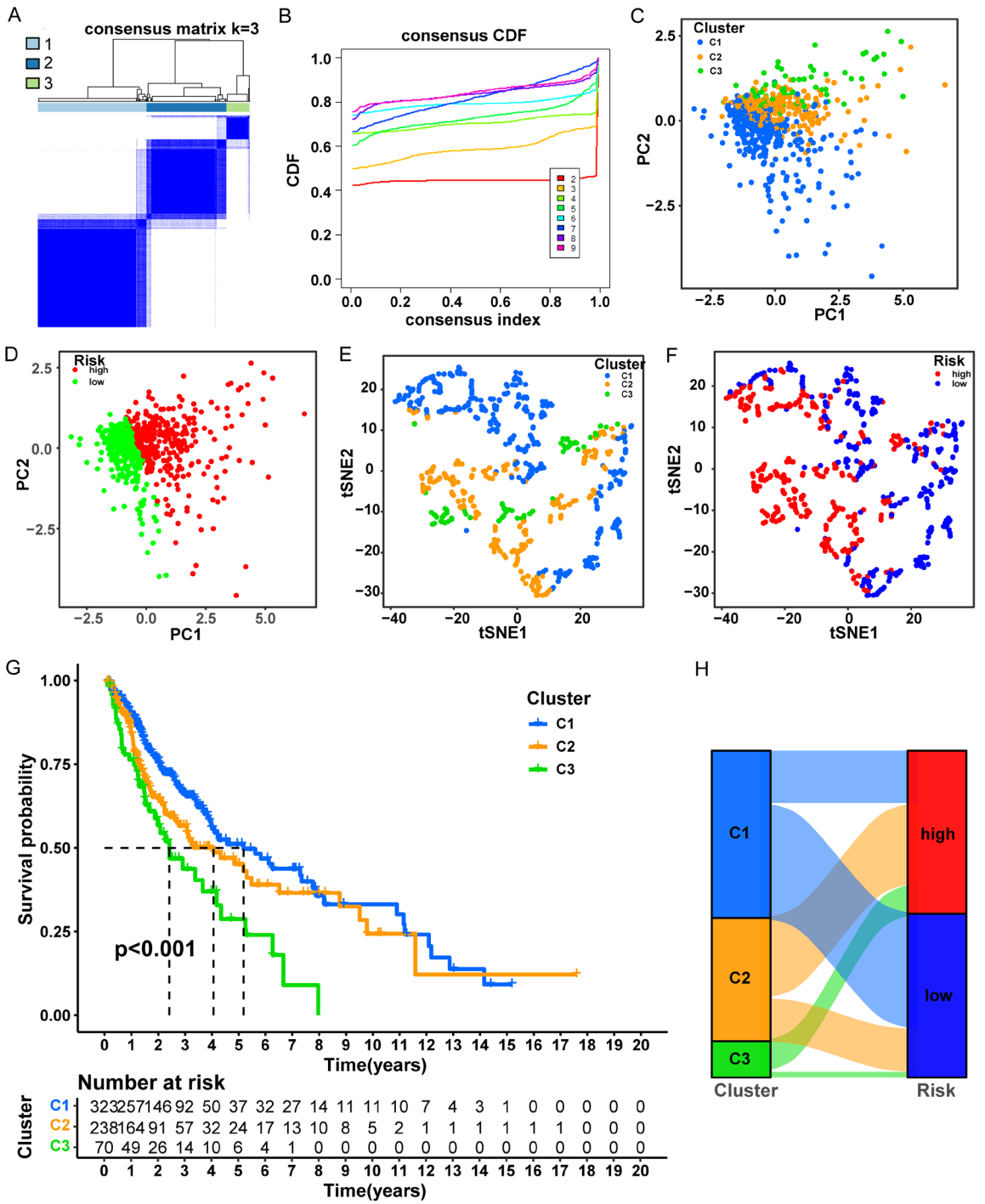

Supplementary Figure 5. Immunogenic cell death-related genes subtypes in gliomas. A, B: Consensus matrix heatmap defining three clusters (k = 3) and their correlation area. C, D: PCA results indicated a significant difference in transcriptional expression between the two isoforms. E, F: The results of tSNE similarly showed that the transcriptional expression of these two genes differed significantly. There was good discrimination between the homozygotes. G: Survival analysis of three Gene clusters. H: Sankey diagram showed the changes in IRGs clusters and gene clusters.

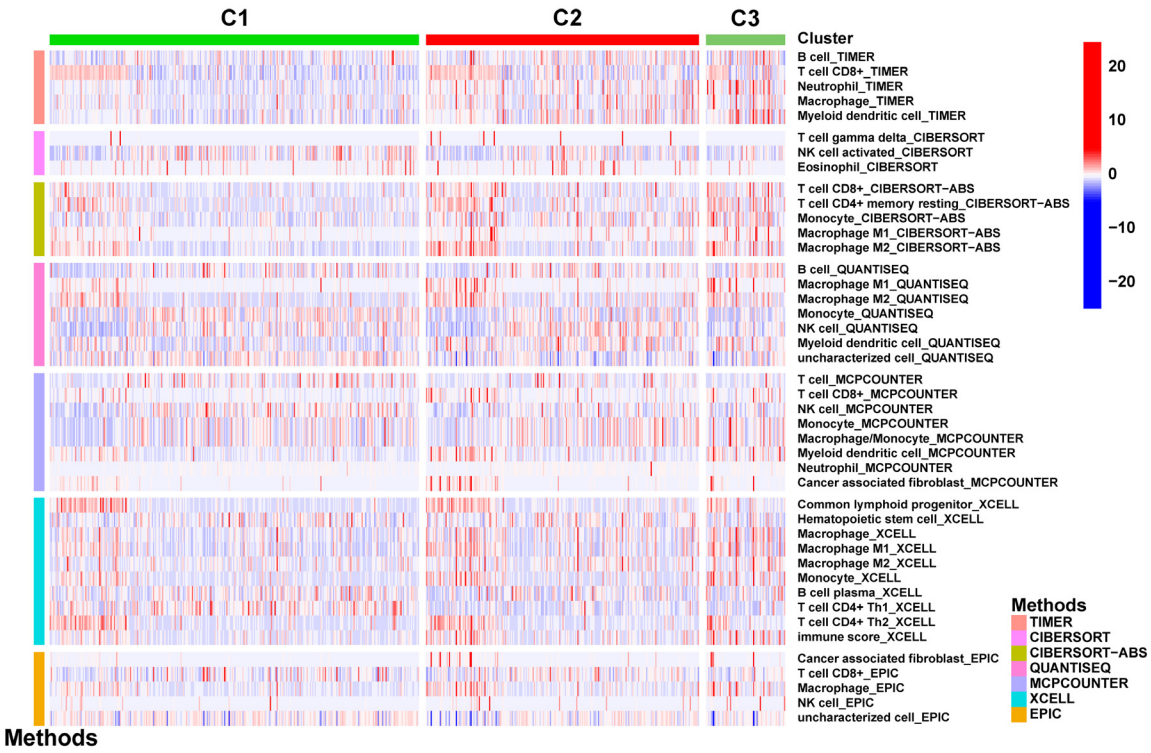

Supplementary Figure 6. Immunoreactive heat maps based on CIBERSORT, ESTIMATE, MCPcounter, ssGSEA, and TIMER algorithms in different molecular subtypes were conducted.

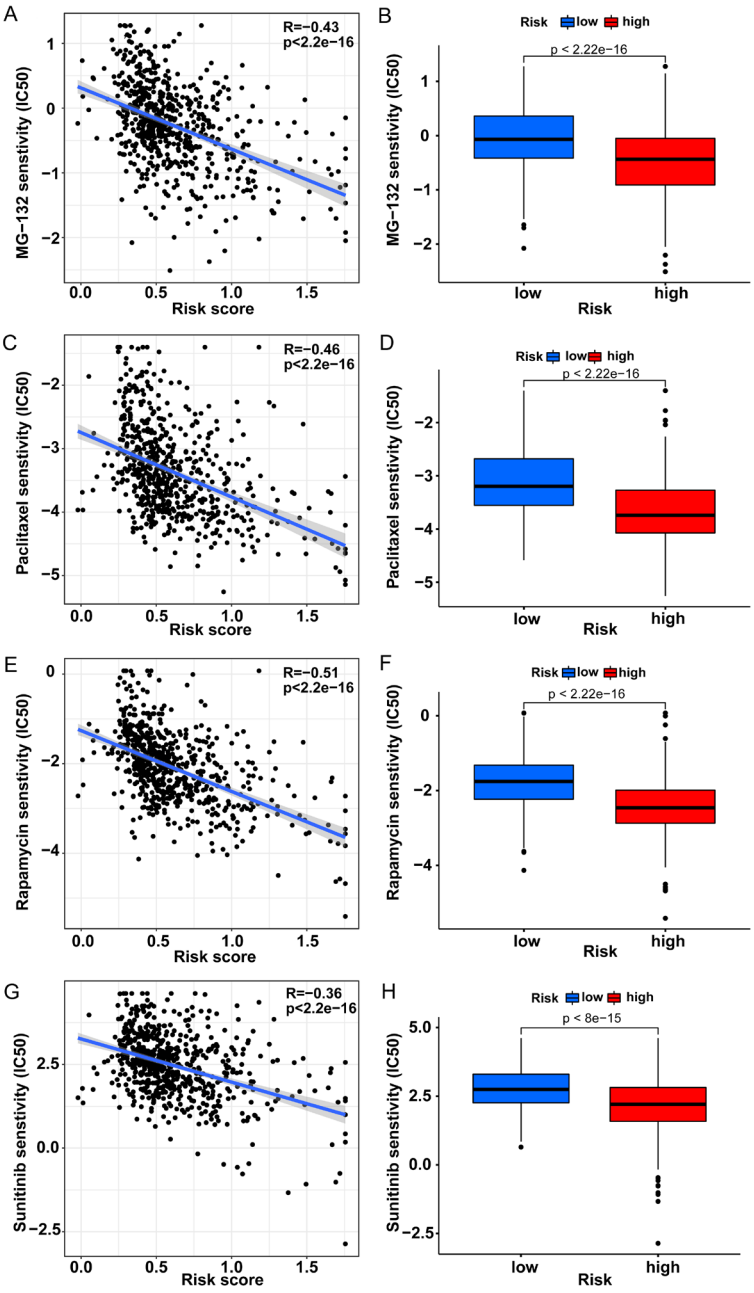

Supplementary Figure 7. A-H: Signature and drug sensitivity correlation analysis.